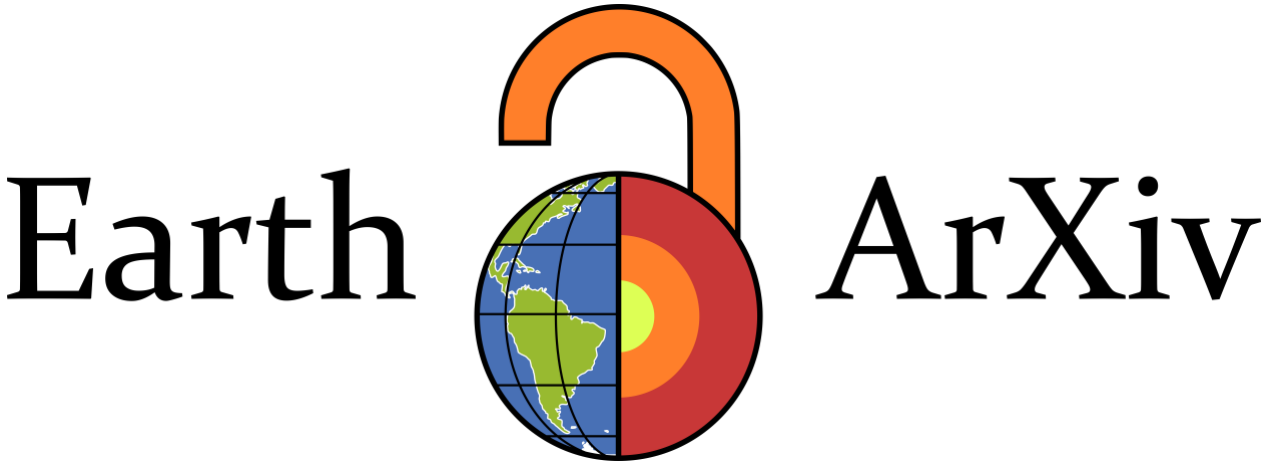

# Future Sea Ice-Ocean and Biological Productivity Changes in the North Water Polynya Region under Policy Relevant Warming Levels

Jed E. Lenetsky,[a] Alexandra Jahn,[a] Patrick Ugrinow,[a] Christopher Wyburn-Powell,[a] Rajan Patel,[a] Hannah Zanowski,[b]

[a] *Department of Atmospheric and Oceanic Sciences and Institute of Arctic and Alpine Research, University of Colorado - Boulder, Boulder, Colorado, USA*

[b] *Department of Atmospheric and Oceanic Sciences, University of Wisconsin-Madison, Madison, Wisconsin, USA*

*Corresponding author*: Jed E. Lenetsky, jed.lenetsky@colorado.edu

ABSTRACT: The North Water Polynya (NOW) is one of the most productive biological regions in the Arctic with high importance to Inuit and local communities of Nunavut and Greenland. To provide insights into the potential changes of this region as global temperatures rise, we investigated the sea ice, and physical and biological oceanic responses of the NOW to low (2°C) and high (>3.5 °C) levels of warming using the Community Earth System Model version 1. As global temperatures increase, we find that sea ice production decreases, spring open water area increases, and that the polynya disappears earlier in the summer as open water areas in the NOW region connect with open water in central Baffin Bay earlier. These sea ice changes contribute to increased stratification, which in turn, leads to increased concentrations of nutrient-rich West Greenland Irminger Waters (WGIW) throughout the NOW region. At low warming levels in the eastern NOW region, the WGIW replenishes the surface with nutrients despite increased stratification, leading to an increase in productivity relative to the historical period along the Greenlandic coastline. In contrast, for high warming in both the eastern and western NOW regions, biological productivity decreases because, despite increased nutrient availability at depth, coastal convection and mixing is unable to counter the increased stratification and bring those nutrients to the surface. Internal variability plays a negligible role in driving these future sea ice and ocean changes, highlighting the importance of limiting global temperature increases to 2 °C or less in order to avoid large changes to the NOW ecosystem.

## 1. Introduction

The North Water Polynya (NOW) is one of the largest and most productive regularly occurring polynyas in the Arctic (Hastrup et al. 2018; Harning et al. 2023). Polynyas are defined as ocean regions of persistently thin or low concentration sea ice cover and are characterized by increased sunlight availability, vertical mixing, and nutrients (Marchese et al. 2017). In the NOW, located in Northern Baffin Bay between northwestern Greenland and Baffin Island, large and early phyoto-plankton blooms help support key Arctic species such as walrus, polar bears, bearded seals, and beluga, bowehead, and narwhal whales (Odate et al. 2002; Tremblay et al. 2002; Heide-Jørgensen et al. 2013, 2016; Marchese et al. 2017). Additionally, little Auk colonies transport nutrients onto land, supporting communities of Arctic land animals such as hares, geese, fox, reindeer, and muskox (Mosbech et al. 2018). Named the Pikialasorsuaq and Sarvarjuaq by the Greenlandic and Canadian Inuit respectively, the NOW has served as important hunting grounds for Inuit and pre-Inuit communities for over four thousand years (Raghavan et al. 2014).

The NOW seasonally forms and is maintained by three processes: 1) the southward advection of sea ice away from the Nares Strait into central Baffin Bay due to northerly winds (Barber et al. 2001b; Dumont et al. 2010; Kwok 2007; Bi et al. 2019), 2) ocean mixing driven by latent heat fluxes and brine rejection from sea ice formation (Melling et al. 2001; Yao and Tang 2003; Mysak and Huang 1992), and 3) sensible heat fluxes from northerly winds and off-shore Ekman transports leading to the upwelling of warm, higher salinity, and nutrient rich West Greenland Irminger Water (WGIW) along the West Greenland Coast (Melling et al. 2001; Burgers et al. 2023). These processes drive the active stage of the NOW, from October through April in which ice production in thin ice regions is ongoing (Tamura and Ohshima 2011; Ren et al. 2022), before leading into the post-polynya (inactive) stage from May until August in which areas of thin ice are the first to melt, leading to early open water areas and hot spots of biological activity surrounded by sea ice (Marchese et al. 2017). The Nares Strait ice arch aids the development of both the active and inactive stages of the NOW, as it reduces the southward transport of thick, multiyear sea ice into Baffin Bay (Barber et al. 2001a; Dumont et al. 2009; Vincent 2019; Ren et al. 2022). Traditionally, the formation of the Nares Strait ice arch was viewed as a prerequisite for the formation of the polynya (e.g. Barber et al. 2001a), but recent years in which the ice arch never or only partially consolidated while the polynya nonetheless formed, have highlighted the importance that ocean

mixing and sensible heat mechanisms play for the formation of the NOW (Moore et al. 2023, 2021; Vincent 2020; Howell et al. 2023). Changes in the Nares Strait ice arch have also coincided with reductions in fall sea ice concentration and growth in Northern Baffin Bay (Ballinger et al. 2022), as well as increasing polynya areas and the number of days when the polynya is present, especially in the fall and winter (Preußer et al. 2015; Stroeve and Notz 2018). Furthermore, annual phytoplankton bloom amplitude in the NOW may have declined between 1998 and 2014, associated with increased surface freshwater content from melting land ice and freshwater import from the Arctic Ocean (Marchese et al. 2017). However, if this observed change is a forced response due to warming or caused by interannual to multi-decadal variability is so far unclear (Marchese et al. 2017).

Throughout the late Holocene (~ 2200 to 1500 years ago), the NOW underwent a period of instability, influencing sea ice cover, stratification, and biological productivity (Koerner et al. 2021; Ribeiro et al. 2021). During this period, stronger northerly winds and storms destabilized the Nares Strait ice arch and increased the import of fresh Arctic surface waters into the NOW region (Koerner et al. 2021; Georgiadis et al. 2020). Increased sea ice import limited open water areas within the NOW region, reducing rates of sea ice formation and brine rejection, which, along with fresher surface waters, increased stratification. In turn, stably stratified surface waters impacted productivity by reducing the availability of nutrients in surface waters (Koerner et al. 2021). Changes in surface stratification also coincided with the increased northward penetration of warm, saline West Greenland Irminger Water (WGIW) into the NOW region, further increasing stratification (Jackson et al. 2021). These past changes in NOW oceanographic and biological regimes were substantial enough to influence the ability of societies to subsist in the region. Abandonment of human settlements 2000 years ago in the NOW region corresponds to this period of polynya instability (Ribeiro et al. 2021), and conversely, periods of human settlement in the NOW region correspond to periods of polynya stability (Grønnow 2016). Thus, understanding how the NOW will change in the future is critical for the assessment and mitigation of climate change impacts in northern Baffin Bay.

Despite the ecological and societal importance of the NOW, projections for the NOW region were only recently examined for the 1981 to 2070 period (Buchart et al. 2022). It was shown that changes in future NOW conditions are likely to mirror those of past warmer climates with a less

stable Nares Strait ice arch, and increased stratification from both increased surface freshwater fluxes and transports of WGIW via the Davis Strait (Buchart et al. 2022). These physical changes result in competing processes: larger northward transports of WGIW lead to increased nutrient availability below the mixed layer while increased stratification reduces the ability of those nutrients to reach the surface (Buchart et al. 2022). Even though this study is a substantial step forward in understanding the impact of climate change on the NOW, key questions remain, specifically in regards to projections of the polynya area and ice production, oceanic conditions after 2070, the impact of changes in the NOW on subregional spatial scales, the role of internal vs external climate variability, and the potential impact of coupled air-sea ice-atmosphere interactions in the NOW.

In the following, we address these outstanding questions about the NOW region, using the Community Earth System Model version 1 (CESM1). We do so in the context of policy-relevant specific warming levels as opposed to emissions pathways or time, following the approach taken in the most recent IPCC report (AR6, see Hausfather et al. 2022). In Section 3a we discuss model - observation agreement and sources of bias in the CESM1. In Section 3b, we explore the future evolution of sea ice conditions in the NOW under low warming and high warming levels, and in Section 3c and 3d, we explore oceanographic changes in the NOW region, focusing on the spring and summer during the post-polynya (inactive) stage, in order to link sea ice changes with changes to physical, chemical, and biological ocean conditions. We demonstrate that, despite relatively homogeneous physical oceanographic responses to climate warming across the NOW region, the biological productivity response to climate warming is non-uniform and non-linear.

## 2. Data and Methods

### *a. Climate Simulations*

In order to understand future changes in the NOW region for different warming levels and in the context of internal variability, we use model output from different ensemble simulations with the fully coupled CESM1-CAM5 at a nominally 1° resolution (Hurrell et al. 2013). Specifically, we use model output from the CESM1-LE (Kay et al. 2015) as well as one of the low-warming ensembles that are branched from the CESM1-LE in 2006 (Sanderson et al. 2017). The CESM1-LE, with 40 members, uses RCP8.5 from 2006 to 2100 while the 2.0 low warming simulations, each with 11 members, use RCP8.5 from 2006 to 2016 before switching to a greenhouse gas forcing designed so

that global temperatures stabilize below 2 °C for at least 20 years before the end of the century (see Sanderson et al. 2017, for further details on the low-warming ensembles). We here use CESM1 output instead of output from the newer CESM2 because of more realistic Arctic sea ice fields in CESM1 (DeRepentigny et al. 2020; DuVivier et al. 2020), as well as the availability of dedicated CESM1 simulations that limit global warming to 2 °C (Sanderson et al. 2017).

Diagnostics for the different warming levels we assess, <2°C (low warming) and >3.5°C (high warming), are obtained from the period 2071–2100 in the low warming 2.0 and CESM1-LE simulations (Fig. 1). The simulated global temperature anomalies for these warming levels are calculated relative to 1850–1879 in the first ensemble member from the CESM1-LE. The historical period is defined as the 30 year period from January 1980 to December 2009, in the CESM1-LE and the observational sea ice data. Note that for the biological productivity analysis, fewer ensemble members than for the physical variables were used, as ocean biogeochemistry was corrupted in members 3–8 in the CESM1-LE (see the known issues on the CESM1-LE project website), which affects both the CESM1-LE and the low warming simulations that were initialized from the CESM1-LE. We also do not include member 1 of the CESM1-LE in analyses of biological productivity due to net primary production values being far outside the range of other members of the CESM1-LE during the historical period.

*b. Polynya definitions*

We defined the NOW region in Northern Baffin Bay from 74°N to 79°N and 280°E to 305°E (see red box in Fig. 2). We use two different diagnostics to assess polynya changes within this region: ice production, based on ice growth during the fall and winter active stage (Tamura and Ohshima 2011; Ren et al. 2022), and extent of open water (polynya area), based on sea ice concentration during the summer inactive stage (Preußer et al. 2015). During the active stage, ice production is calculated as the combined monthly ice production ($km^3$) across both frazil and non-frazil ice categories within the CESM1 sea ice model.

For the post-polynya stage, the polynya area is calculated as the sum of the area of grid cells within the polynya region with a sea ice concentration (SIC) below 70%, which we used as a threshold for the presence of open water, following Preußer et al. (2015). Following previous studies that differentiate between the presence of a polynya and continuous open water in northern Baffin Bay

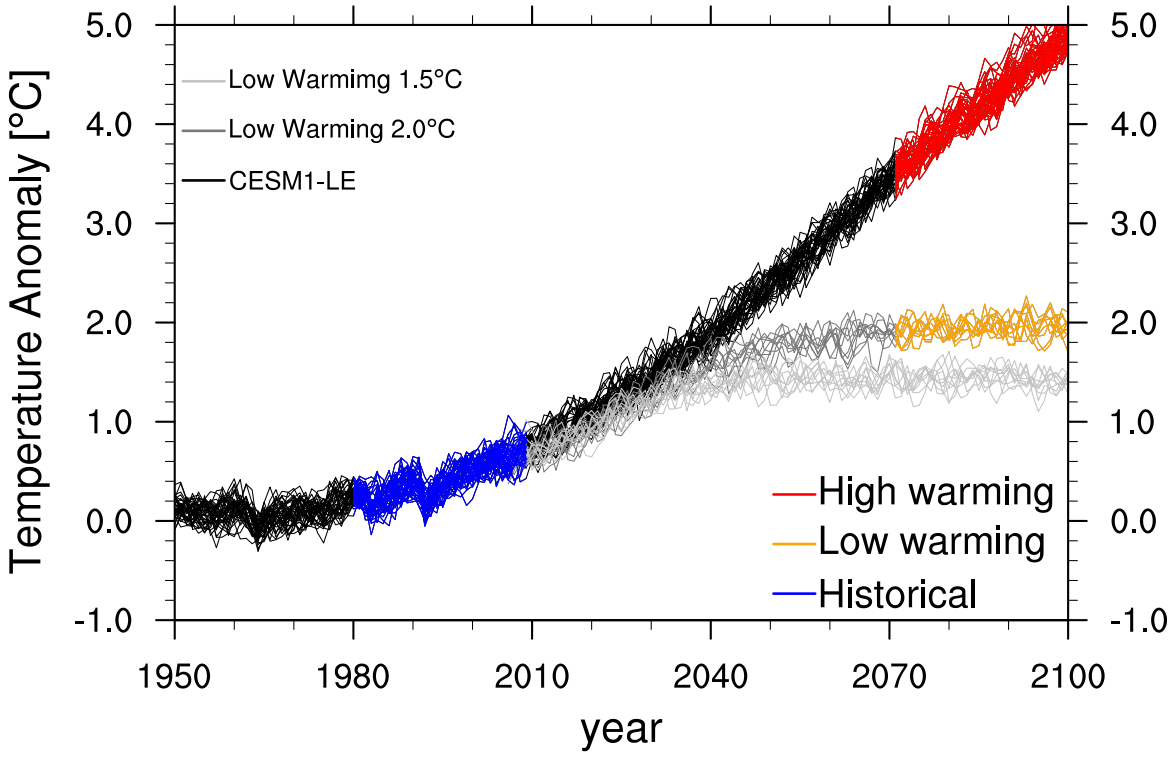


134 FIG. 1. Temperature anomalies relative to 1850-1879 from member 1 of the CESM1-LE (Kay et al. 2015)
135 from the simulations used. In black, the CESM1-LE, and in greys the Low Warming Ensembles for 2°C (darker
136 grey) and 1.5°C (lighter grey; Sanderson et al. 2017). The periods from these simulations that are used are
137 shown in blue for the historical period, orange for low warming, and red for high warming. Details on the global
138 temperature anomalies for the different warming levels can be found in Table S1.

151 (e.g. Dunbar and Dunbar 1972; Barber et al. 2001b), we define a second region in eastern, central
152 Baffin Bay from 72°N to 74°N and 295°E to 305°E (yellow box in Fig. 2). When the average
153 SIC there is less than 50% in this southern region, the NOW is considered to be connected to the
154 Baffin Bay open water region, with no polynya present (i.e., polynya area is 0). Conversely, when
155 the majority (>50%) of this southern region is covered in sea ice, any open water within the NOW
156 region is considered to be closed and isolated from open water further south, and thus part of the

polynya. The choice of this southern SIC threshold does not affect the polynya in the winter and spring, but does affect the timing and magnitude of the polynya's peak area and its dissipation and formation in the summer and fall (Fig. S1). Note that the use of this second region can artificially lower the values of polynya area climatologies by averaging areas of open water when the polynya is present with areas of zero when the polynya is not present (see July in Fig. 3b).

In order to understand the spatial variability of changing ocean conditions within the NOW region, we also define an ocean section across the NOW (76.2°N, 280 - 289.5 °E) and examine ecological changes at one eastern location (76.2°N, 289°E) and one western location (76.5°N, 283°E) along the section (see Fig 2). The results presented are insensitive to the exact choice of the eastern and western locations.

To assess the ability of the CESM1 to simulate the present-day NOW polynya during the inactive stage, polynya areas calculated from the historical simulation are compared to observed polynya areas calculated from monthly NOAA/NSIDC Climate Data Record of Passive Microwave Sea Ice Concentration (SIC), version 4 (Meier et al. 2021).

### *c. Ice fluxes*

In order to assess the contribution of sea ice from the central Arctic Ocean on sea ice conditions in the NOW, we define the Nares Strait ice area flux (IAF) as:

$$IAF = \int_L (SIC * V_{ice}) dL \tag{1}$$

where SIC is the sea ice concentration, $V_{ice}$ is the meridional sea ice velocity, orthoginally crossing the Nares Strait northern gateway at 292.2 - 295.6°E and 82.6°N (Fig. 2), and $L$ is the length of the gateway (127 km). The results presented are insensitive to both the location of the gateway in northern versus southern Nares Strait. We also compare simulated sea ice area fluxes during the historical period with satellite observations for 1997-2009 (Kwok et al. 2010) and 2016-2019 (Moore et al. 2021) based on available datasets.

We also assess solid freshwater fluxes as the sum of sea ice and snow on sea ice freshwater equivalents through the Nares Strait and southern NOW (74°N; 285:300°E) as

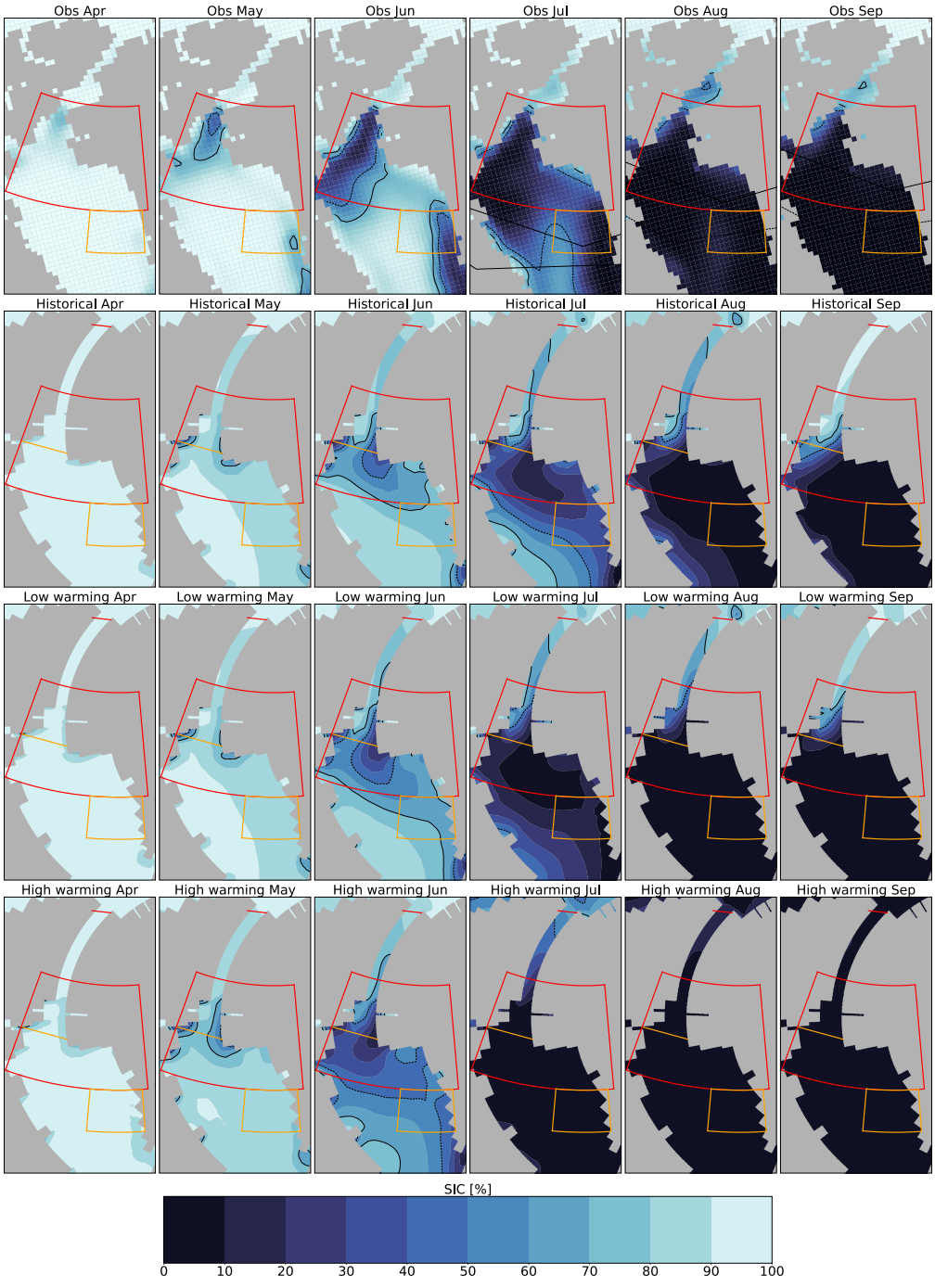


171 FIG. 2. Observational and ensemble mean May, June, July, August, September, and October sea ice concen-
172 trations (SIC) in Northern Baffin Bay from the NSIDC observational passive microwave record (Meier et al.
173 2021) for the historical period 1980-2009 (first row), and the CESM1 for the historical period (second row), low
174 warming (third row), and high warming (bottom row). The North Water Polynya (NOW) region is outlined in red
175 and the southern region is outlined in yellow. The 70% SIC contour is outlined in a black solid line and the 50%
176 SIC contour is outline in a black dashed line. The approximate location of the northern Nares Strait gateway is
177 shown in red and location of the NOW ocean cross section used in Figs. 8 & 9 is shown in orange.

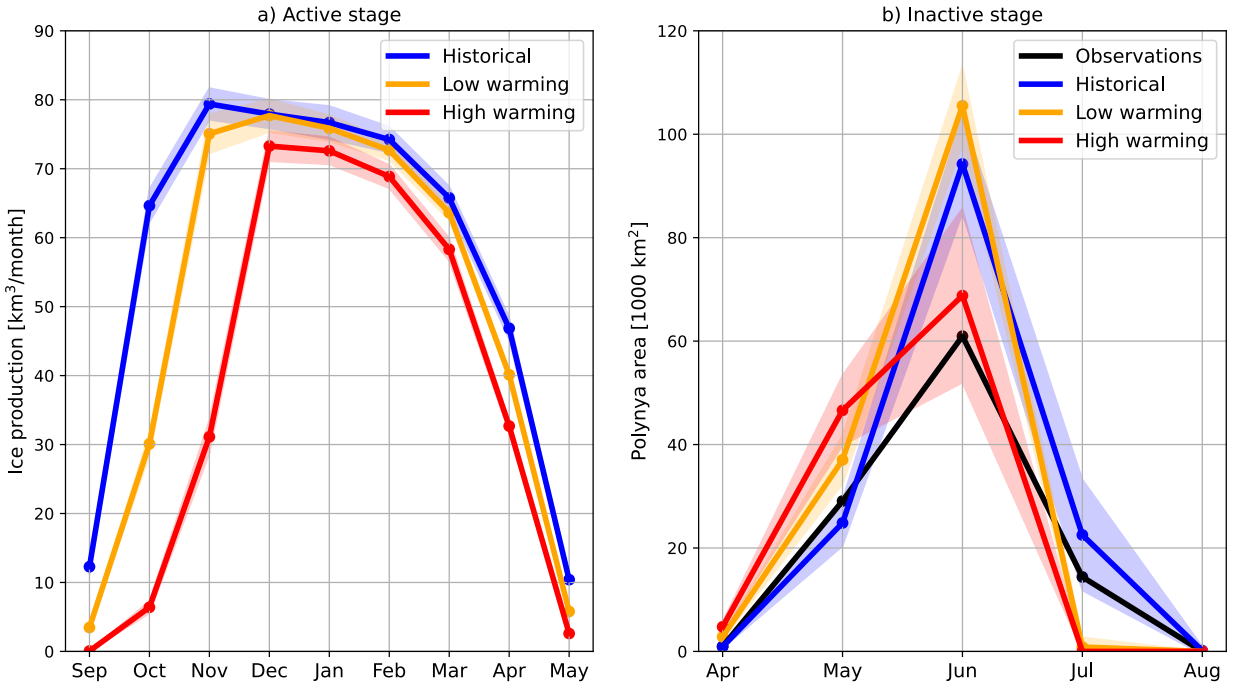


FIG. 3. Changing seasonal cycle of polynya ice production during the active stage (a) and and polynya area during the inactive stage (b), from observations (inactive only; 1980-2009; black), CESM1-LE historical (1980-2009; blue), low warming (yellow), and high warming (red) levels. Shading indicates ± 1-standard deviation from the ensemble mean.

$$FFW_{solid} = \frac{\rho_{ice}}{\rho_{fw}} \int_H \int_L \frac{S_{ref} - S_{ice}}{S_{ref}} (SIC * V_{ice}) dLdH + \frac{\rho_{snow}}{\rho_{fw}} \int_H \int_L (SIC * V_{ice}) dLdH \quad (2)$$

where H is the thickness of the layer, $S_{ref}$ is reference salinity (34.8 g/kg), $S_{ice}$ is sea ice salinity (4 g/kg), and $\rho_{snow}$, and $\rho_{fw}$ are the densities of sea ice (917 kg/m$^3$), snow (330 kg/m$^3$), and pure freshwater (1000 kg/m$^3$) respectively.

### *d. Assessment of stratification*

In order to quantify vertical changes to ocean density in the NOW under different warming levels, which can influence nutrient availability and biological productivity, we define buoyancy content ($B$; Schmidt and Send 2007):

$$B = -\frac{g}{\rho_0}\int_0^h [\rho(z) - \rho(h)]dz \tag{3}$$

where g is gravitation acceleration, $\rho_0$ is reference density of 1025 kg/m$^3$, and $\rho(h)$ is the potential density at the base of the ocean layer with thickness $h$. $B$, similarly to other metrics such as available potential energy (Gjelstrup and Stedmon 2024; Polyakov et al. 2018), is a vertically integrated measure of stratification, and represents the energy required to remove vertical density gradients and fully mix the water column from the surface to depth $h$. Furthermore, following Schmidt and Send (2007), we can use the linearized equation of state, $\rho = \rho_0(1 - \alpha\Delta T + \beta\Delta S)$, to estimate the relative contributions of temperature and salinity to $B$:

$$B \approx B_T + B_S \tag{4}$$

$$B_T = g\alpha\int_0^h [\Theta(z) - \Theta(h)]dz \tag{5}$$

$$B_S = -g\beta\int_0^h [S_A(z) - S_A(h)]dz \tag{6}$$

where $\Theta$ is the conservative temperature, $S_A$ is the absolute salinity, and $\alpha$ and $\beta$ are the thermal expansion and haline contraction coefficients respectively. In the following, we calculate $B$, $B_T$, and $B_S$ over the upper 55 and 155 meters of the water column in order to assess both near surface and deeper changes to stratification. The results presented are insensitive to the exact choice of $h$.

## 3. Results

### *a. Modelled North Water Polynya over the historical period*

The simulated seasonal cycles of the polynya diagnostics (ice production and area) are qualitatively very similar to the observed seasonal cycle over the historical period during all seasons (Fig. 3), with the the seasonal cycle of simulated sea ice production rates agreeing with observational estimates in terms of both regionally averaged magnitude and seasonal cycle (Tamura and Ohshima 2011; Ren et al. 2022). The active stage of the NOW begins in September when ice growth begins, peaking in November at $\sim 80$ km$^3$/month of sea ice growth and slowly declining until May when ice growth ceases (Fig. 3a). Simulated ice production rates are underestimated in the model by $\sim 15$

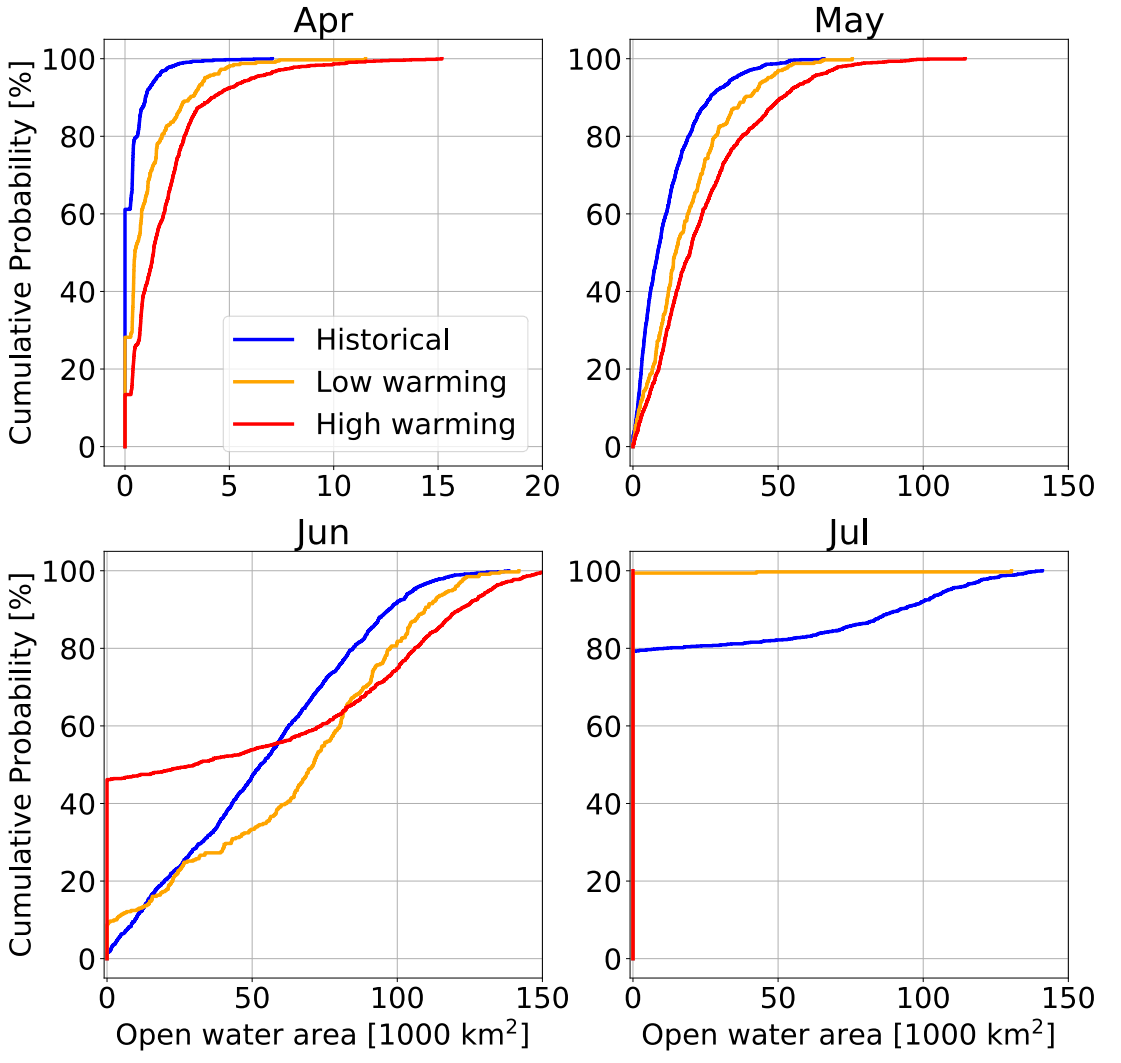


212 FIG. 4. Cumulative probability of open water areas [in 1000 km$^2$] from CESM1-LE historical (1980-2009;
213 blue), low warming (orange), and high warming (red). Note the different x-axes on each of the panels, due to the
214 different polynya areas for April compared to May through July.

228 m/year compared to published observed rates (Tamura and Ohshima 2011); however, this is likely
229 due to differences in the definitions of the NOW region. In the inactive post-polynya stage from
230 May to July, simulated polynya areas during the historical period agree quite well with satellite sea
231 ice observations, except for a substantially larger peak area in June (Fig. 3b). After the inactive

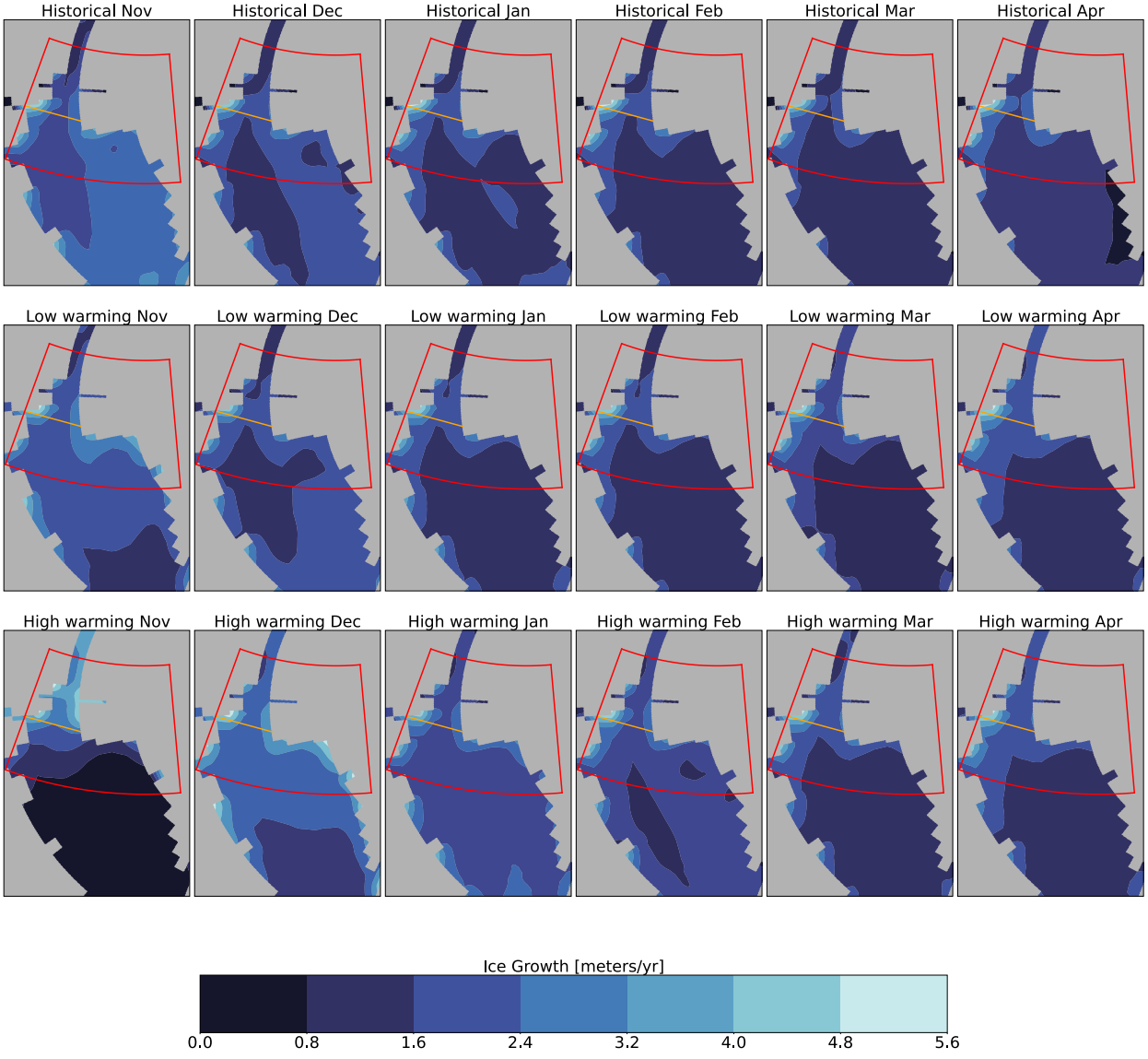


FIG. 5. Ensemble mean November, December, January, Fabruary, and April sea ice growth rates in Northern Baffin Bay the simulated historical period 1980-2009 (first row), low warming second row), and high warming (bottom row). The North Water Polynya (NOW) region is outlined in red and the location of the NOW ocean cross section used in Figs. 8 & 9 is shown in orange.

polynya peaks in June, the seasonal retreat of sea ice in Baffin Bay begins to reduce SIC south of the NOW region, connecting the NOW to the open waters of northern and central Baffin Bay (Fig. 2). As a result, even though open water is still increasing in the NOW region in July (Fig S1), the 30-year average polynya area in July declines as the NOW ceases to be a polynya in several years

and becomes open water instead (Fig 4). Thus, non-zero polynya areas less than the June peak in July reflect primarily internal variability in sea ice conditions south of the polynya, as opposed to changing sea ice conditions within the NOW region.

Despite the good agreement on the seasonal cycle of the polynya ice growth and area, the spatial ice growth and SIC in the NOW region in spring differs between the CESM1 and observations (Fig. 2 & 5). This difference is most likely primarily due to the absence of a Nares Strait sea ice arch in the CESM1, resulting in simulated historical ice area fluxes that have a different seasonal cycle and are larger than observed fluxes in the spring and summer over the 1997-2009 period (Fig. 6a; Kwok et al. 2010). The simulated seasonal cycle of Nares Strait sea ice fluxes over the historical period shows a late fall and winter minimum rather than a minimum in spring, and hence shows a much earlier increase in the simulated sea ice area fluxes after the seasonal minimum. Furthermore, the similarity in solid freshwater transports between Nares Strait and southern Baffin Bay (Fig. 6c-d), is in disagreement with observations that show that Nares Strait sea ice transports do not substantially contribute to sea ice transports in southern Baffin Bay (Howell et al. 2024). Despite high winter and spring sea ice concentrations (SIC > 85%), monthly mean sea ice velocities magnitudes in the Nares Strait are too large (> 0.1 cm/sec) to be considered slow pack ice according to Laliberté et al. (2018), suggesting that the ice arch would still be missing in CESM1 even with the inclusion of updated landfast ice parameterizations (e.g. Lemieux et al. 2016; Sterlin et al. 2024). As a result, we conclude that in the CESM1, large Nares Strait sea ice areas fluxes are due to a combination of the course model resolution that is unable to resolve the narrow passages of the Nares Strait interior, and weak internal ice stresses (despite high sea ice concentrations) that are unable to adequately resist wind stress (Dumont et al. 2009). Note that in higher resolution CESM1 simulations, Nares Strait ice area fluxes still show an opposite seasonal cycle compared to Kwok et al. (2010), peaking in spring instead of fall (Fol et al. 2025), suggesting that model resolution alone cannot explain biases in ice area transports.

The impact of the differences in the simulated and observed Nares Strait sea ice flux is most apparent on sea ice growth rates during the fall and winter, when ice growth rates are reduced compared to observations and regions of sea ice growth are only present on the eastern and western margins of the NOW south of Nares Strait (Fig. 5), as opposed to in the central channel as seen in observations (Tamura and Ohshima 2011; Ren et al. 2022). These discrepancies in ice growth rate

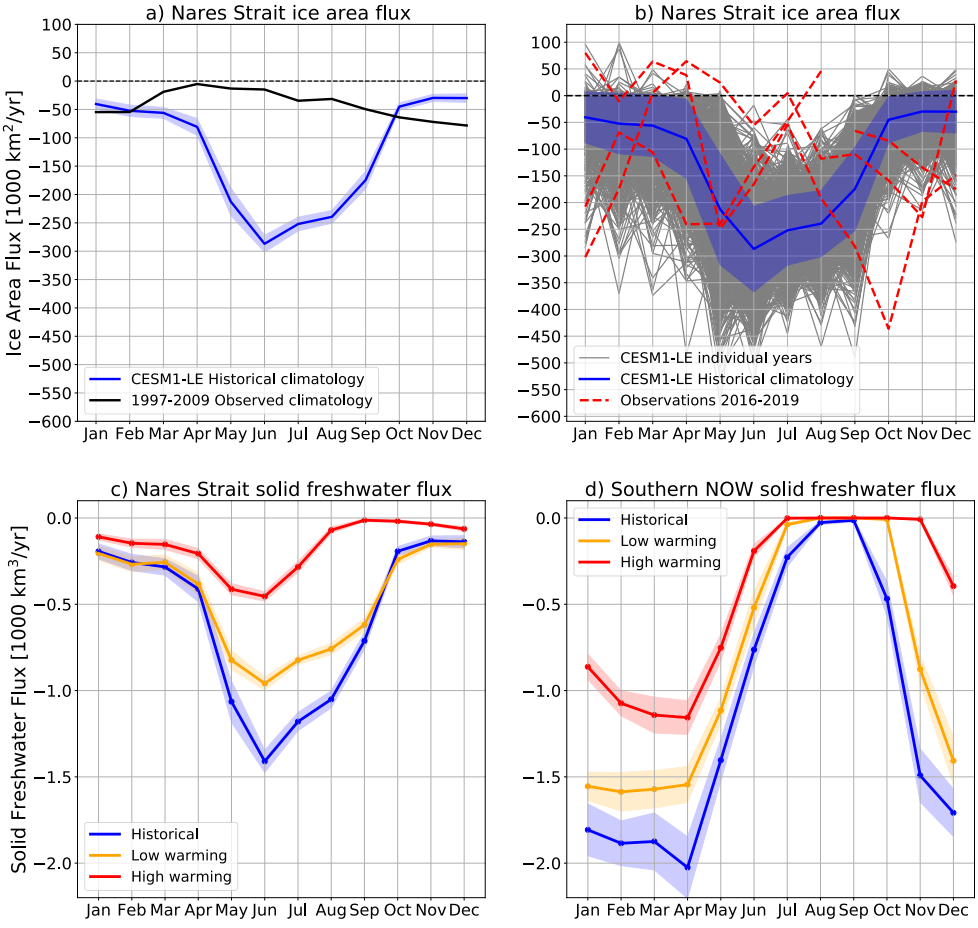


FIG. 6. Seasonal cycles of sea ice area and solid freshwater fluxes in the NOW region. Negative values indicate southward fluxes. Panel a) shows the observed climatology of ice area fluxes from 1997-2009 across the northern Nares Strait (Kwok et al. 2010) in black, and the simulated climatology over the CESM1-LE historical period (1980-2009). Blue shading indicates ± 1-standard deviation from the ensemble mean climatology. Panel b) again shows the simulated ice area flux climatology in blue over the historical period, along with individual annual cycles for each year and member from the CESM1-LE historical period in grey. Blue shading indicates ± 1-standard deviation of annual cycles across all years and members. Available years of recently observed ice area fluxes from years (2016-2019; Moore et al. 2021) when the ice arch was less stable are shown in red dashed lines. Observational uncertainties are small at approximately 4.4 1000 km$^2$/yr (Moore et al. 2021). Panels c) and d) show solid freshwater fluxes through Nares Strait (c) and southern NOW region (d) for historical (blue), low warming (orange), and high warming levels (red), with shading indicating ± 1-standard deviation from the ensemble mean climatology.

and spatial pattern are consistent with the steady inflow of pack ice through Nares Strait, insulating the ocean surface and limiting the exchange of turbulent heat with the atmosphere, which in turn, inhibits sea ice growth (Fig. S2; Mysak and Huang 1992; Melling et al. 2001; Yao and Tang 2003). Key differences are also present in the April and May SIC (Fig. 2), when the observations show approximately 10-30% lower SIC and a polynya forming south of Nares Strait while the simulated polynya is confined to the coastlines. This spatial difference is due to ice being advected by northerly winds to the south from away from Greenland and Ellesmere Island, as opposed to away from an ice arch in the central channel. In June, the much larger simulated Nares Strait sea ice area flux in the CESM1 is also clearly apparent in the spatial SIC, with a relatively high SIC tongue extending into northern Baffin Bay in the CESM1 (Fig. 2). Nonetheless, the CESM1 simulates a large polynya across the NOW region in June, in agreement with data from more recent years that show that the NOW polynya formed despite no Nares Strait ice-arch forming (Moore et al. 2021, 2023). In terms of the effect of biased ice area fluxes on future projections of open water area and ice production in the NOW region, we expect the lack of an ice-arch to have less of an effect than for historical conditions, as the recent frequent breakdowns or failures to form an ice-arch while the NOW still formed (Moore et al. 2023), as well as observational studies (Kirillov et al. 2022) and climate simulations (Fol et al. 2025), suggest that the ice-arch will exist less frequently or potentially not at all in the future. In fact, when simulated historical ice area transports through the northern Nares Strait are compared to more recent years when the ice arch was less stable (Moore et al. 2021), the seasonal cycles show somewhat better consistency in terms of magnitude, with key differences remaining in phase (Fig. 6b). For example, in May 2018 and May 2019, when the ice arch was not present, the resultant observed ice area fluxes agree with the simulated May historical climatology, but then decreased in the summer and increased in the fall to levels outside the range of simulated climatology. While it is difficult to draw strong conclusions from comparisons between a 30 year climate model ensemble and four years of observations, this stronger agreement of the CESM1 ice fluxes with more recent observations suggests that simulated ice area fluxes are not unrealistically large in the absence of a stable ice arch. Thus, future Nares Strait sea ice fluxes are likely to exhibit stronger agreement with simulated ice transports in a warmer climate.

Another source of spatial differences in the regions of open water in the post-polynya stage is likely biases in the simulated atmospheric circulation. In the CESM1-LE, the 10-meter wind field

climatology over the historical period (Fig. 7) shows a similar circulation pattern and seasonal cycle to ERA-5 winds, with the strongest northerly winds in the winter and spring and the weakest in the summer. However, there are some key differences, such as an approximately 2 m/s wind speed bias in the western NOW south of Nares Strait as well as a wind speed maximum located within the Nares Strait as opposed to south of the strait in ERA-5. Importantly, it has been shown that to resolve all details of the effect of atmospheric forcing on the sea ice - ocean interface in the NOW region, model resolutions below 10 km are needed (Moore and Våge 2018; Gutjahr and Heinemann 2018; Moore 2021; Moore and Imrit 2022; Kohnemann and Heinemann 2025). As a result, the approximately 66 km atmosphere (50 km ocean-sea ice) resolution for CESM1, and 17 km for ERA-5, are both too coarse to capture extreme wind events due to ageostrophic intensification from along-strait pressure gradients and steep topography of the Nares Strait, which play a key role in modulating surface fluxes in the NOW region (Moore 2021; Gutjahr and Heinemann 2018; Barber et al. 2001a). Note that the CESM1 resolution is the standard resolution of current state-of-the-art climate models, so coupled global model simulations at the required less than 10 km resolution are currently not available. In sum, these biases suggest that in CESM1, the influence of oceanic oceanic sensible heat processes are likely overestimated, while turbulent heat fluxes and ice advection play a lesser role due to biases in ice area fluxes and winds. Nonetheless, despite the challenges described above, the agreement with the observed seasonal cycle of polynya area and ice production lends confidence to use the CESM1 to provide an estimate of the expected large scale oceanographic changes that may occur within the NOW region over the 21st century, in particular for June and July (which show stronger agreement with observations), based on the currently available global, fully-coupled, large ensemble climate simulations.

*b. Projected future changes in North Water Polynya ice production and area*

As atmospheric warming increases, the polynya has a larger area during the spring due to both reduced sea ice growth and import through Nares Strait during the cold season, helping to precondition a thinner ice cover for an earlier and more expansive spring and summer melt. Decreases in NOW ice production are most pronounced in October and November (Fig. 3), in agreement with recent observational studies in Baffin Bay and modeling studies of Antarctic polynyas, which attribute these changes to surface ocean warming from advected ocean heat

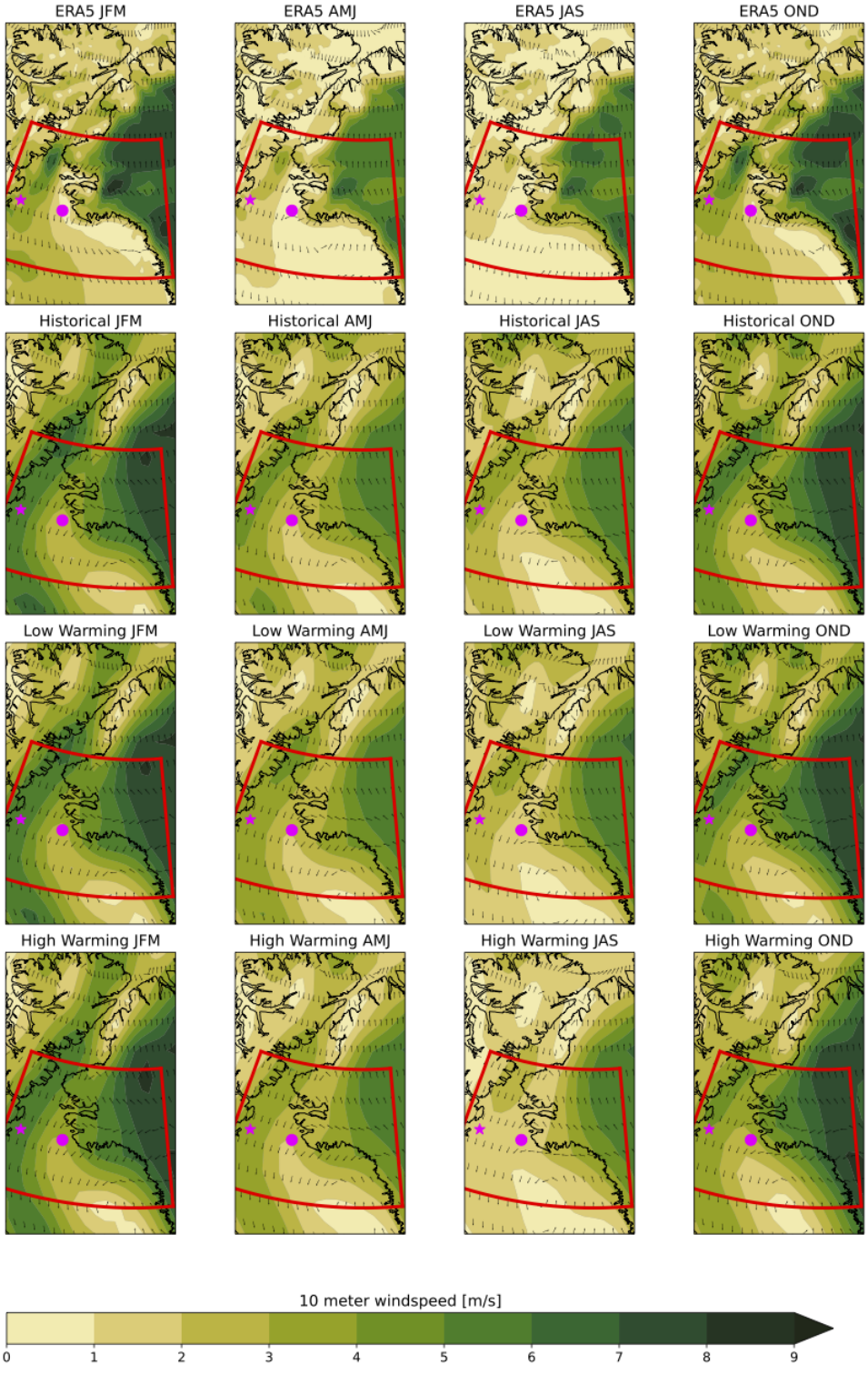


330 FIG. 7. Spatial map of the 10 meter atmospheric circulation during winter (JFM), spring (AMJ), summer
331 (JAS), and fall (OND) over the NOW region in ERA5 over the historical period (1980-2009), and CESM1 over
332 the historical, low warming, and high warming levels. The extent of the NOW region is shown in red, and the
333 location of ocean section and East and West locations are shown in magenta.

transports and enhanced ice-albedo feedback (Ballinger et al. 2022; Jeong et al. 2023a). Under low warming, fall ice growth progresses more slowly and peaks a month later than under historical conditions, but still matches December historical conditions at its peak. Under high warming however, the entire sea ice growth season is shortened by a month, and the December peak growth is $\sim 7$ km$^3$ lower than the November historical peak, driven by minimal ice growth in the southern NOW region (Fig. 5). There are minimal warming level differences in regionally averaged ice growth rates in the winter and spring months, as the sea ice thickens in the winter, reducing vertical heat fluxes, and air temperatures begin to warm in the spring (Fig. 3 & S2). Changes to ice growth with warming level are also accompanied by decreases to solid freshwater import from Nares Strait into the NOW region and reduced solid freshwater export from the southern NOW region into central Baffin Bay (Fig. 6c-d). These changes to winter ice growth, and sea ice import and export act to thin the winter sea ice cover and accelerate spring sea ice melt and the opening of the polynya. In April, the ensemble mean polynya areas are over 2-3 times larger for low warming and 5 times larger for high warming warming compared to the historical period (Fig. 3). Viewed in the context of internal variability, the likelihood of spring open water areas enlarging increases (Fig.4). For example, in April, the likelihood of open water areas within the NOW being below the arbitrary threshold of 5000 km$^2$ decreases from $\sim$ 100% under historical conditions to $\sim$ 98% under low warming, and $\sim$ 91% under high warming (Fig. 4). In May, a similar pattern occurs, with increases in both average and anomalous polynya areas with warming (Fig. 3 & Fig. 4).

In summer, the NOW area increases with warming when it exists as a polynya. Specifically, in June, the ensemble mean polynya areas are largest for low warming levels and decrease below historical levels under high warming (Fig. 3). This is because in more than 40% of June cases for high warming levels, the open water in the NOW region is connected to open water in southern Baffin Bay and as a result, the polynya is not considered to be present (see Fig. 4 and Fig. S1). However, when the polynya is present for high warming levels in June, the polynya area is larger compared to lower warming scenarios due to more extensive spring melt (Fig. 4). In July, the probability of the polynya disappearing and becoming connected to open waters in southern Baffin Bay further increases with climate warming. In the historical period, there is a 80% chance that the polynya will not exist in July compared to a 99% chance for low warming, and 100% of the time for high warming (Fig. 4). In summary, global temperature increases are associated with more

extensive sea ice melt and larger polynya areas in the spring, as well as an increased likelihood of polynya disappearance in June and July.

*c. Projected future changes in oceanographic conditions*

Increasing open water and polynya areas in the NOW region are accompanied by increased stratification in the surface ocean due to warming and freshening. Across the NOW ocean section (see Fig. 2 for its location) in May, waters remain at the freezing point at low warming levels and see slight warming in the western section for high warming levels (Fig. 8). Surface salinities across the section are approximately 2.5 g/kg fresher at high warming than historically, and 1.5 g/kg fresher compared to warming of <2 °C (Fig. 9). These differences in surface salinity for different warming levels persist throughout the melt season. For surface temperatures, warming level differences do not emerge until later in the summer in July and August, when increases in surface temperatures compared to the historical period can range from 4-6 °C for high warming levels. The effect of these salinity and temperature changes can be seen in the earlier emergence and deepening of the 25.0 $\sigma_\theta$ isopycnal (solid line; Fig. 8 & 9). In the historical period, waters this light are not present in the NOW region until August, and then only in the uppermost 15 meters. As warming increases, this layer of water appears earlier in the summer and deepens: arriving in July for low warming levels down to 24 meters, and for high warming levels deepening from 46 meters in May to below 80 meters in August. Changes in stratification can also be viewed in terms of buoyancy content (Section 2d), with summer and fall buoyancy increasing with warming levels over the upper 55 meters in the west, east, and total NOW region (Fig. 10a-c). For low warming levels, upper ocean buoyancy content is driven almost entirely by vertical salinity gradients ($B \approx B_S$), whereas under high warming levels, increased stratification is driven by both by both vertical temperature and salinity gradients ($B \approx B_S + B_T$), highlighting the role of upper ocean warming on stratification throughout the NOW region.

Substantial changes are also seen in oceanographic conditions at depth between historical and future periods, namely the warming and salinification of waters below the 27.0 $\sigma_\theta$ isopycnal (dashed line; Fig. 8 & 9). This isopycnal is strongly sloped across the NOW region due to northerly winds and offshore Ekman transport along the west Greenland coast (Melling et al. 2001; Burgers et al. 2023). In the NOW region during the historical period, temperatures and salinities are relatively

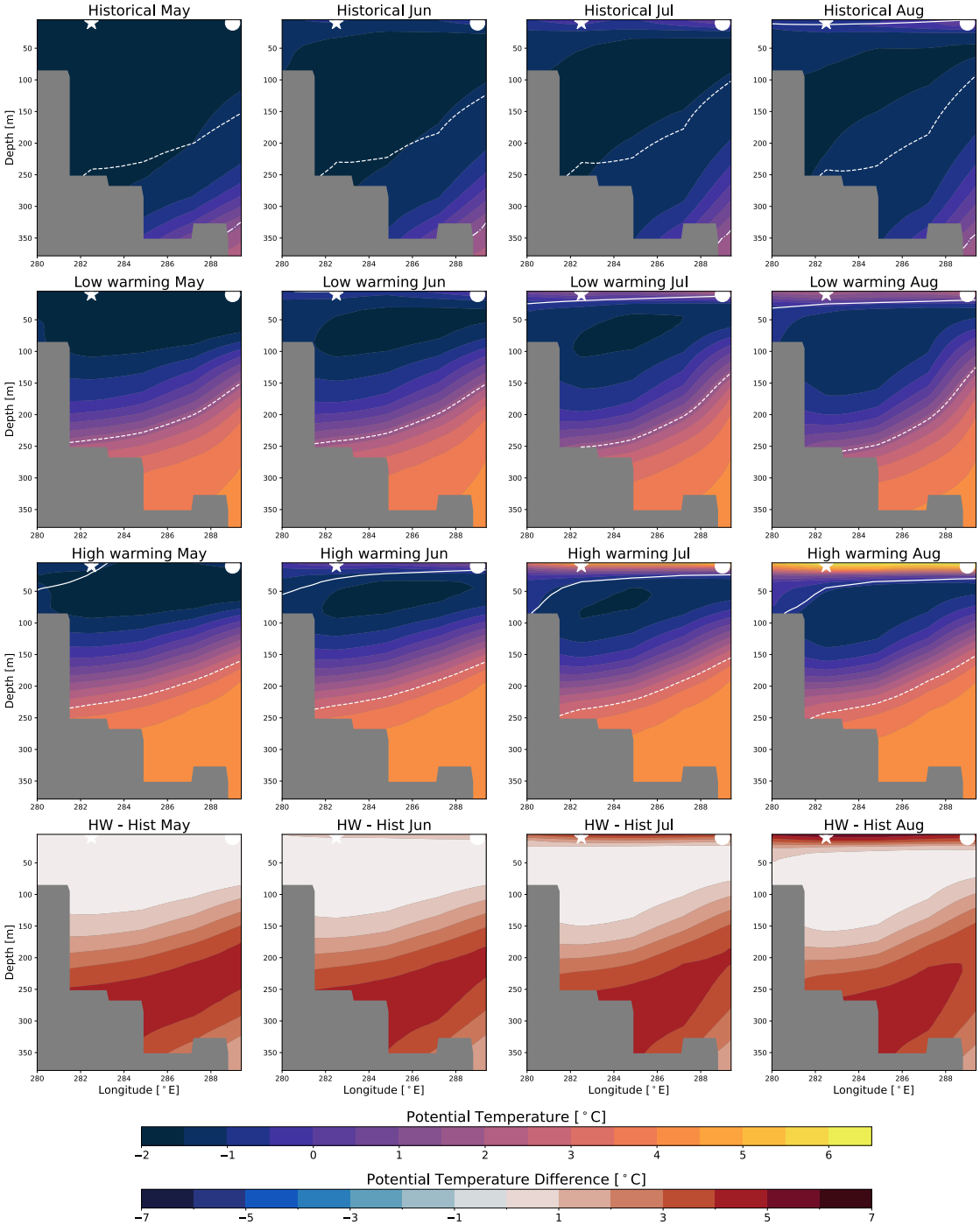


FIG. 8. Cross section of potential temperature along 76.2 °N across the NOW region (see Fig. 2 or 11 for the location of the section) for May through August for historical, low warming, and high warming warming levels. The 25.0, 27.0, and 27.5 $\sigma_\theta$ isopycnals are shown in solid, dashed, and dashed-dotted white lines respectively. The bottom row shows the difference between the high warming level and historical period. The location of the east and west points used for NPP assessment in Fig. 12 are shown as white star and circle respectively.

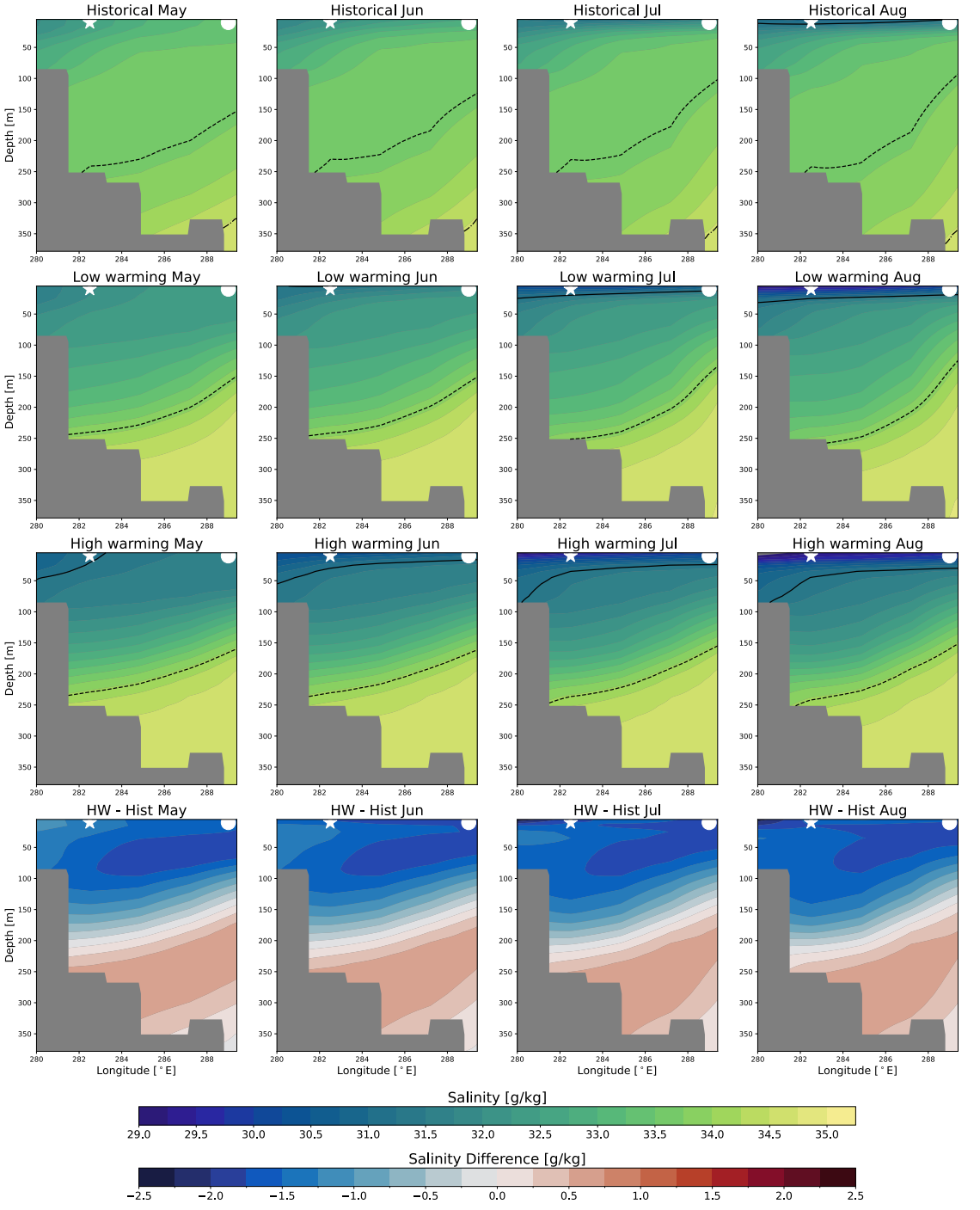


FIG. 9. Cross section of salinity along 76.2 °N across the NOW region (see Fig. 2 or 11 for the location of the section) for May through August historical, low warming, and high warming warming levels. The 25.0, 27.0, and 27.5 $\sigma_\theta$ isopycnals are shown in solid, dashed, and dash-dotted black lines respectively. The bottom row shows the difference between the high warming level and historical period. The location of the east and west points used for NPP assessment in Fig. 12 are shown as white star and circle respectively.

constant between 50 and 200 meters before increasing with depth. Additionally, in all months of the historical period, cold, salty, waters denser than 1027.5 kg/m$^3$ are present in at depth in the eastern section in all months (dashed-dotted line; Fig. 8 & 9). The presence of these deep saline waters is in agreement with hydrographic surveys which suggest that while warm, saline WGIW may travel northward into the NOW region before recirculating southwards, WGIW is largely limited to the southern margins of the NOW and can lose much us its heat in transit to the NOW (Melling et al. 2001; Münchow et al. 2015). For all warming levels, however, an increase in temperature and salinity is observed, particularly below 27.0 $\sigma_\theta$ isopycnal, associated with the shoaling and northward penetration of warm WGIWs into the NOW region, as well as the disappearance of waters denser than 1027.5 kg/m$^3$. This watermass redistribution at depth, contributes to increased stratification throughout the NOW region (Fig. 10d-f) over the upper 155 meters, the approximate depth of the 27.0 $\sigma_\theta$ isopycnal in the eastern NOW, by increasing vertical salinity gradients, despite warmer temperatures at depth partially counteracting the stratification in some regions ($B_S > B$). Increased WGIW at depth is likely due to both increased transports of WGIW into Baffin Bay via the Davis Strait (Castro de la Guardia et al. 2015), as well as an increased transport of WGIW from northern Baffin Bay into the NOW region. An enhanced northward penetration of WGIW into the NOW region is supported by paleoclimate proxies from a warmer climate with a less stable ice arch, increased stratification and reduced brine formation, decreasing densities at depth (Jackson et al. 2021). Importantly, the depth of the 27.0 $\sigma_\theta$ isopycnal does not substantially change with warming, due to the replacement of cold, fresh waters by warmer, saline waters, rendering the mid-depth vertical density structure largely unchanged, and keeping WGIW accessible to the surface mixed layer via upwelling.

### *d. Future projections of biological conditions*

Despite stratification increasing in-step with increasing warming levels, biological productivity responds non-linearly and non-uniformly. At all warming levels and the historical period, primary production begins in April and May within areas of enhanced sea ice melt on the eastern and western coastal regions of the NOW (Fig. 11 & 12a-c), where exposure of the surface mixed layer to increasing seasonal levels of sunlight leads to a bloom that lasts until August when the seasonal decline in nutrients coincides with a decline in sunlight (Fig. 10g-i; Marchese et al. 2017). In the

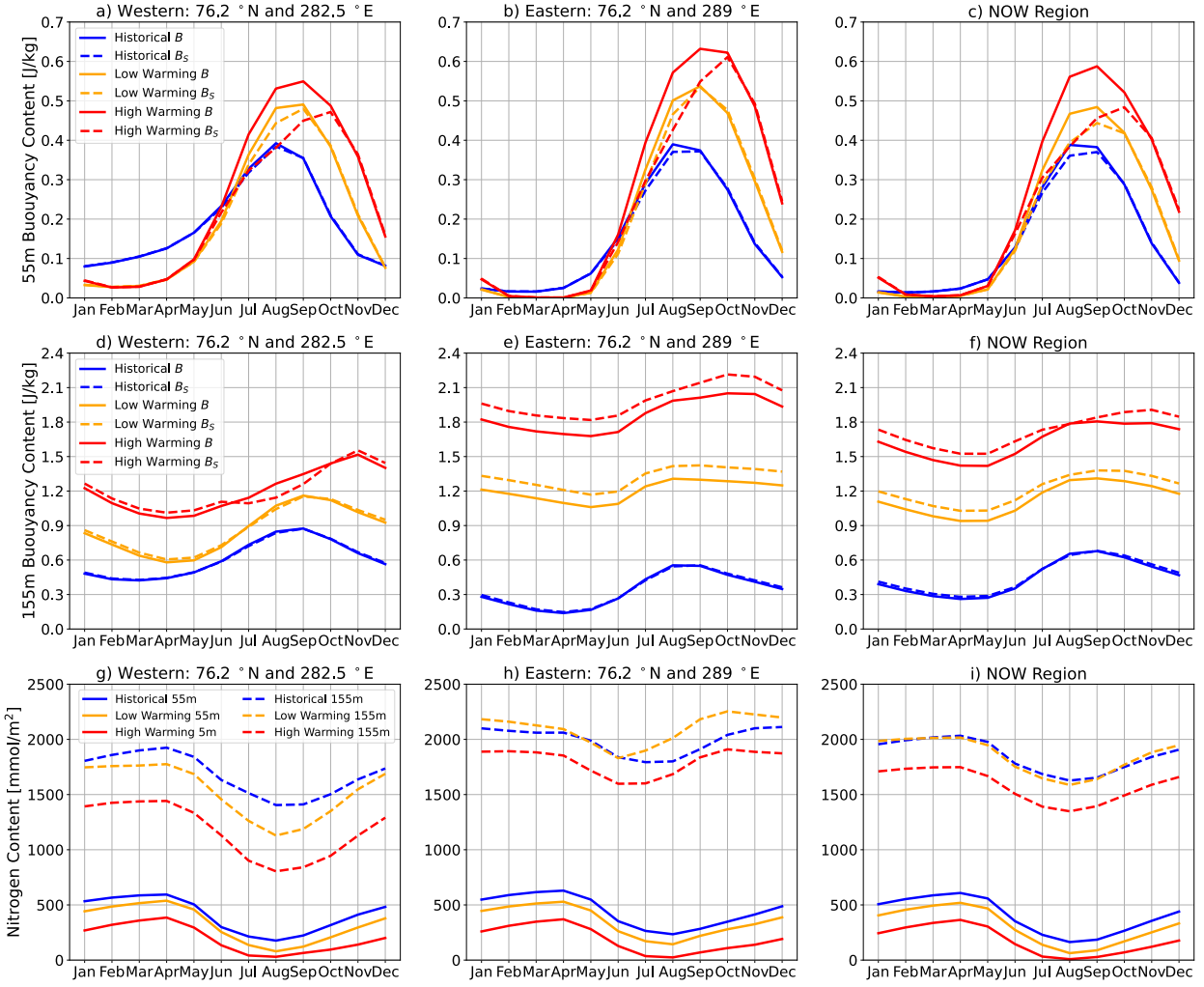


FIG. 10. Buoyancy content for upper 55 meters for a) western, b) eastern, c) NOW region and upper 155 meters for d) western, e) eastern, f) NOW region. Dashed lines show contributions of salinity to buoyancy ($B_S$) and solid lines show contributions of both temperature and salinity ($B$). Vertically integrated nitrate content g) western, h) eastern, f) NOW region over upper 55 meters (solid line) and 155 meters (dashed line).

eastern NOW region, July and August productivity increases for low warming levels by ~20% (Fig. 12b). This increase in productivity for warming below 2 °C is due to both declining SIC which exposes more of the ocean surface to sunlight, warming surface temperatures that can increase phytoplankton growth rates (Kirillov et al. 2022; Wolf et al. 2024), and the northward penetration of WGIW into this region, which, due to predominantly upwelling favorable northerly winds, leads to an enhanced nutrient supply to the surface mixed layer compared to the historical period, despite an increase an increase in stratification (Fig. 10h). This increase in productivity is partially

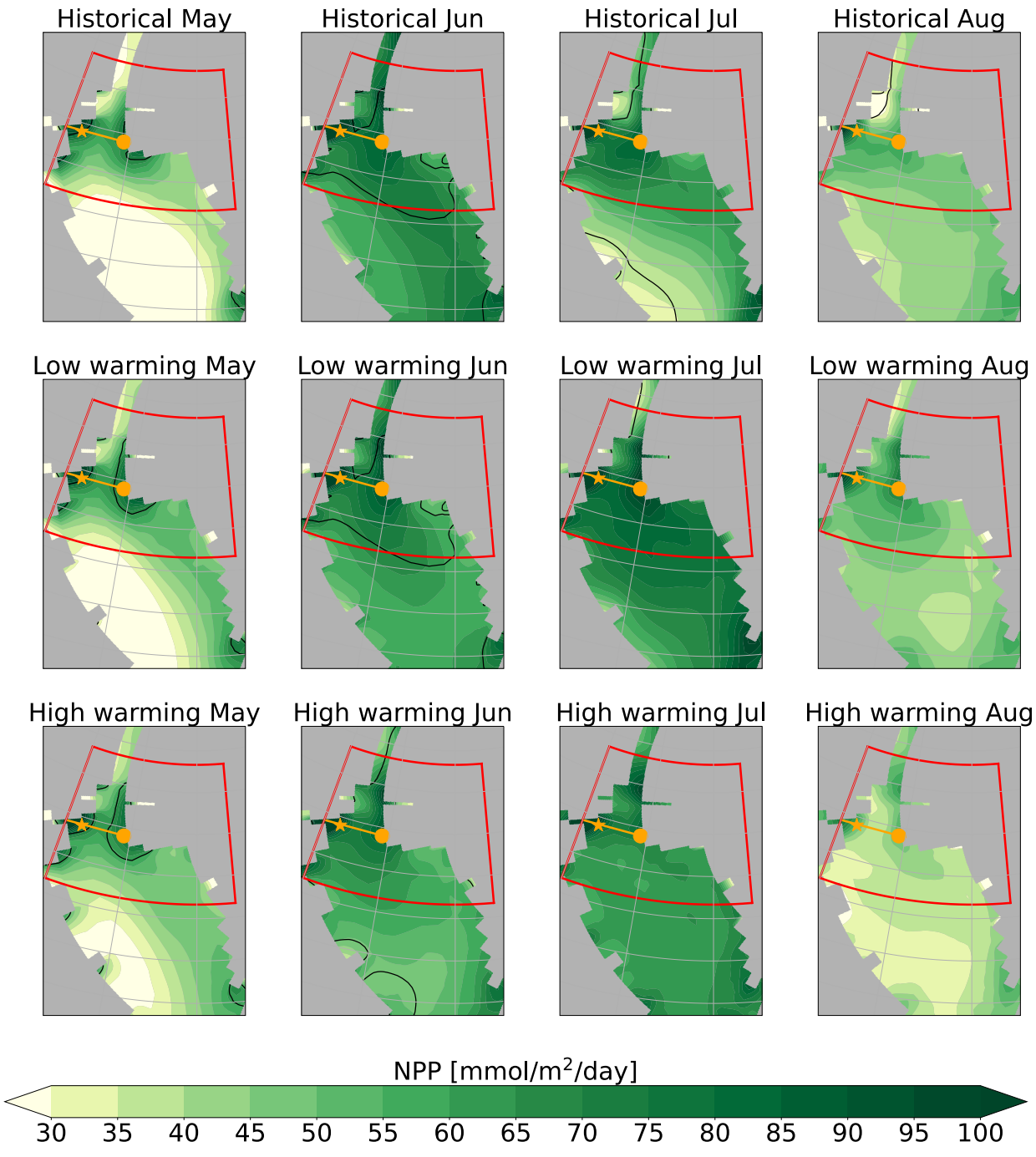


436 FIG. 11. Spatial map of ensemble mean net primary productivity (NPP) for May through August for the
437 historical, low warming and high warming warming levels. The NOW section is shown in orange, with the
438 position of the eastern location marked with a orange dot and the position for the western location marked with
439 a orange star. Black line shows the 70% SIC contour. The red box shows the NOW region.

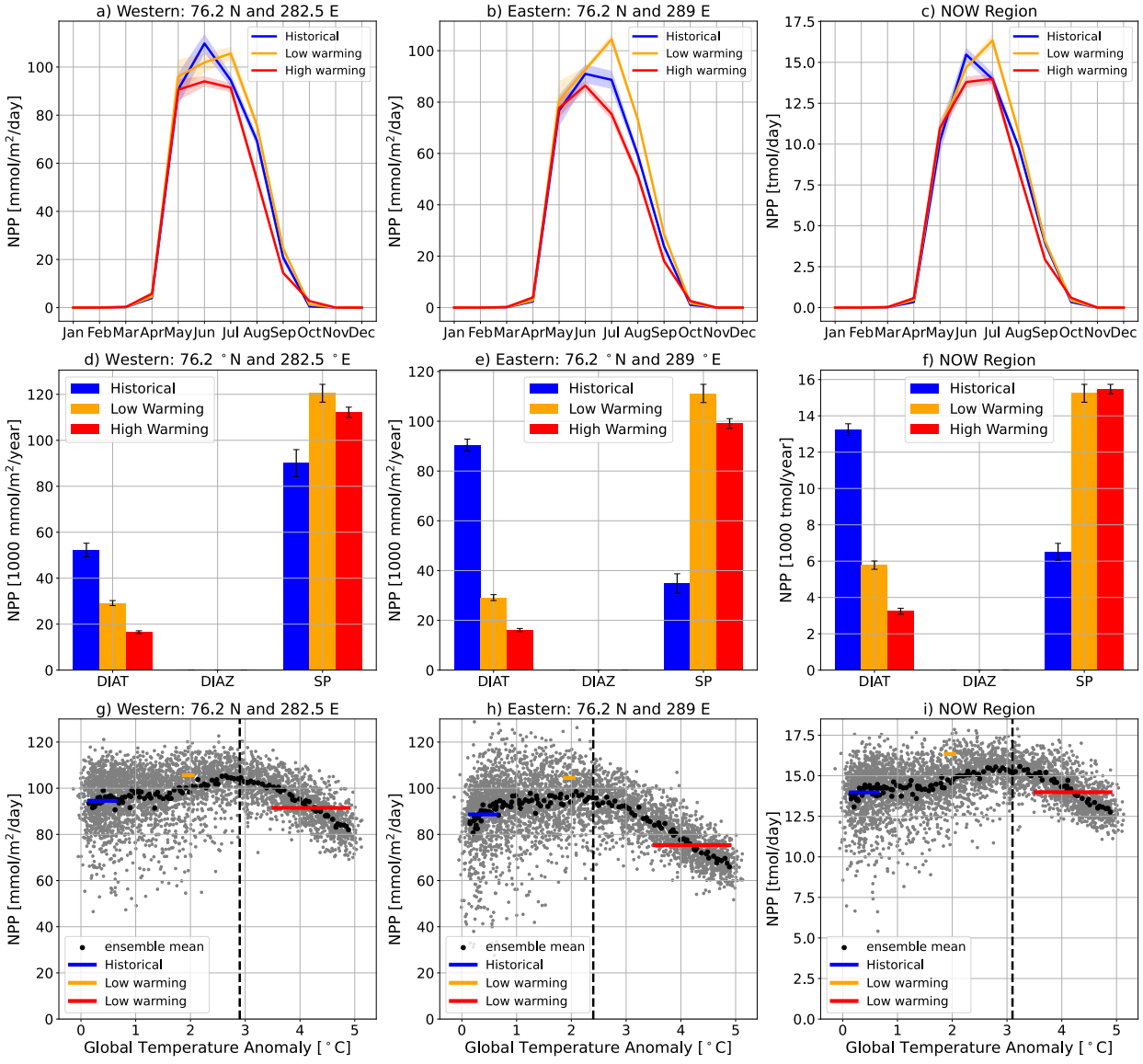


FIG. 12. Top row: Seasonal cycle of ensemble mean net primary productivity (NPP) for historical, <1.5 °C, <2 °C and >3.5 °C warming levels at the a) western location, b) eastern location, and c) total NOW region (see Fig 11 for precise positions). Shading indicates ± 1 standard deviation of seasonal cycles between ensemble members. Middle row: annual total NPP by phytoplankton type for diatoms (DIAT), diazotrophs (DIAZ), and small phytoplankton (SP) for historical, low warming, and high warming levels at the d) western location, e) eastern location, and f) total NOW region. Error bars indicate ± 1 standard deviation of annual totals. Bottom row: July NPP vs warming level for the entire CESM1-LE simulation from 1980-2100 at the g) western location, h) eastern location, and i) total NOW region (see Fig. 11). Ensemble mean NPP values are shown in black and individual ensemble members are shown in grey. Average July NPP values based on the 30yr ensemble mean historical, low warming, and high warming levels are shown in blue, orange, and red respectively. The vertical dotted black line shows the transition point when NPP begins to decline based on segmented linear regression analysis.

driven by a shift in phytoplankton community composition from one dominated by diatoms to one dominated by small phytoplankton (Fig. 12e). While both small phytoplankton and diatoms are primarily limited by nitrogen in the spring and summer (Moore et al. 2013), small phytoplankton out-compete diatoms in nitrogen poor environments, and are thus better able to take advantage of increases in temperature and available sunlight in comparison to diatoms, leading to an increase in peak NPP despite increased stratification under low warming levels (Marinov et al. 2010; Moore et al. 2013). For high warming levels, however, July and August total NPP declines by ~15% below historical levels across all phytoplankton groups because coastal upwelling is no longer able to overcome the even greater surface stratification, so nutrients can not be replenished after the early season bloom (Fig. 10h & 12). In the high productivity region in the western NOW, peak NPP remains similar to historical levels for low warming levels, but with a shift in the peak from June to July (Fig. 12a). The lack of increasing peak productivity in the west compared to the east is due to both downwelling-inducing dominant winds (Fig. 7) and a deeper and more diluted WGIW layer, so that in the western part of the NOW there is no enhanced nutrient supply from below for low warming levels (Fig. 10g). Similar to the eastern NOW, stratification is associated with diatom populations declining in favor of small phytoplankton under all warming levels, as well as peak NPP under high warming declining by 14% compared to the historical period (Fig. 12). When integrated over the entire NOW region (Fig. 12c), the seasonal cycles of productivity also show a shift in peak productivity from June to July with increasing warming levels, with a slight increase in peak productivity for low warming. There is also a decline in annually integrated productivity by ~5% compared to historical levels for high warming, substantially less than the declines in annual productivity of 10% and 8% in the west and east, respectively, for the same warming level. This is due to the partial compensation of the decline in the highest productivity regions in the east and the west of the NOW under high warming by a small increase in productivity in the Nares Strait due to declining SIC (Fig. 11). In summary, if warming exceeds 2 °C, annual mean productivity in the NOW is projected to decrease by 5% and local peak productivities are projected to decrease by as much as 15%, along with a substantial shift in phytoplankton community composition.

## 4. Discussion

We find that non-linear changes in biological productivity in the NOW in a warming climate are associated with reduced cold season ice growth, reduced sea ice import and export, larger spring open water areas and earlier polynya disappearances, and driven by the balance between increases in surface stratification, changes in phytoplankton community composition, and nutrient availability at depth. For all both investigated warming levels, surface freshening in the NOW region is driven by a combination of changes in sea ice melt, runoff, and Arctic Ocean freshwater export through Nares Strait. Previous work with the CESM1 (Jahn and Laiho 2020), and other climate models (Rasmussen et al. 2011; Zanowski et al. 2021), have shown that Nares Strait liquid freshwater fluxes are projected to increase and solid fluxes are predicted to decrease with climate warming, supporting the increases in stratification seen at low and high warming levels. Despite biases in Nares Strait ice area fluxes during the historical period, the agreement between CESM1 and more recent ice area flux observations (Moore et al. 2021) lends confidence to our future projections of solid freshwater import into the NOW, as well as its downstream impacts on stratification in the NOW and freshwater transports to southern Baffin Bay (Fig. 6). While CESM1 does not include a coupled ice-sheet model, simulated runoff also increases with warming level (Fig. S3), and, along with freshwater from the Nares Strait and local sea ice melt, provides an additional source of freshwater to promote increased stratification, in agreement with other modeling studies that explicitly prescribe glacial discharge (Buchart et al. 2022). However, the influence of glacial meltwater on biological conditions in the NOW is a source of uncertainty. It is possible that the additional glacial freshwater input could reinforce stratification and further reduce nutrient transport to the surface mixed layer (Buchart et al. 2022); Or, freshwater plumes from basal melt could entrain nutrients and provide an additional mechanism for nutrient delivery to the surface despite increased stratification (Kanna et al. 2018). Furthermore, given the uncertainties associated with both ice area fluxes and glacial meltwater, a sensitivity study using a high-resolution fully coupled, ocean–sea ice–ice sheet model, with updated sea ice stress and landfast ice parameterizations (Lemieux et al. 2016; Sterlin et al. 2024), should be carried out to assess these questions in the future. In short, despite the uncertainty related to Baffin Bay freshwater inputs, this study highlights the key roles that both long-range Arctic freshwater export and local runoff and sea ice melt plays in modulating physical and biological oceanographic conditions in the NOW region.

We identify three distinct sea ice–ocean regimes in biological productivity in the highest productivity regions in the NOW: a historical regime, low warming regime, and a high warming regime. In the historical regime, stratification is minimal, as surface waters are cooler and more saline, and less WGIW at depth results in a relatively uniform water column. This vertical structure promotes mixing and high rates of biological productivity (Marchese et al. 2017; Hastrup et al. 2018). Ocean conditions in the low warming regime are associated with surface warming and freshening, as well as increased surface stratification and concentrations of nutrients and WGIW at depth. Despite the increased stratification, productivity in the low warming regime is greater than or equal to productivity in the historical regime due to higher nutrient availability, warmer temperatures (Wolf et al. 2024), and changes in phytoplankton community composition (Marinov et al. 2010). Furthermore, increased polynya and open water areas expose more of the ocean surface to wind stress, helping to promote upwelling events that can overcome the surface stratification and resupply the mixed layer with nutrients (Tremblay et al. 2011; Rumyantseva et al. 2015). In the high warming regime, productivity in the eastern and western regions is reduced compared to the historical regime because northerly wind stresses are not able to overcome the even greater stratification. As a result, the key differences between the low and high warming regime, as well as the sign of productivity changes in the eastern and western NOW, depend on whether or not wind-induced upwelling is strong enough to overcome the stratification and resupply the mixed layer with nutrient-rich WGIW. Importantly, northerly winds in the NOW region remain at a consistent magnitude under both low and high warming levels, suggesting that potential changes to the regional atmospheric circulation, and its influence on upwelling in the western NOW, cannot explain the projected ocean changes between the historical, low, and high warming regimes (Fig. 7). Although projections of the atmospheric circulation and air-sea interactions are source of uncertainty due to the coarse model resolution (Moore and Våge 2018; Gutjahr and Heinemann 2018; Jeong et al. 2023b), our findings of minimal changes to atmospheric circulation are in agreement with other modeling studies which found negligible changes to wind stress in northern Baffin Bay (Muilwijk et al. 2024). Note that the total and eastern NPP seasonal cycles for low warming levels, as well as all high warming NPP seasonal cycles, exhibit changes outside the ensemble spread of historical seasonal cycles (Fig. 12a-c). As a result, we can conclude that changes between the different ocean states underlying

these productivity regimes are driven by external forcing (warming level), as opposed to internal climate variability.

An analysis using segmented linear regressions across the CESM1-LE from 1980 to 2100 shows that the transition between low and high warming regimes occurs at approximately 2.9, 2.4, and 3.1 °C for the western, eastern, and total NOW regions, respectively (Fig. 12g-i). The warmer transition point in the total NOW region, compared to the east and west, is in agreement with Buchart et al. (2022) who found that regionally averaged NPP in the NOW only weakly responded to climate warming. The higher regional versus local sensitivity to climate warming also adds to a body of work highlighting the importance of sub-regional spatial scales in the NOW region (Bailey et al. 2013). Even in the presence of spatial SIC biases due to coarse model resolution, we have confidence in these sub-regional differences in biological productivity, as they are based on the underlying simulated ocean circulation and watermass distributions, which are supported by both historical observations (Tang et al. 2004; Burgers et al. 2023) and paleoclimate proxies (Jackson et al. 2021). Importantly, due to model biases and uncertainty on the strength of future Arctic storms (Nishii et al. 2015; Day et al. 2018), the exact temperature thresholds associated with these biological regimes are a source of uncertainty. Notably, productivity is higher in the dedicated low warming simulations compared to the ensemble mean NPP from the CESM1-LE forced by RCP8.5 at the same warming level (Fig. 12g-i). These differences suggest that the NOW will respond differently to a given short lived climatic state when warming is continuously increasing (transient) versus when a global temperature anomaly is constant. The reduced forced response and high internal variability of biological productivity when continuous climate warming is below 1.5°C (Fig. 12i) can help contextualize observed changes in the NOW region, and indicates that observed declines in peak phytoplankton bloom amplitudes in the NOW region are most likely due to internal variability and not climate warming (Marchese et al. 2017). Furthermore, the NPP response for transient vs constant temperature anomalies can further help explain why this study sees a stronger response in NPP to climatic warming compared to Buchart et al. (2022), who used transient (RCP 4.5 & 8.5) greenhouse gas forcings. In summary, dedicated, policy relevant, low-warming climate simulations demonstrate that keeping warming to below 2 °C is likely to maintain the NOW region as a key Arctic ecosystem with high biological productivity. Under less than 2 °C globally, NPP

is expected to be similar to or higher than during historical conditions, but shifts in phytoplankton community composition should be expected.

## 5. Conclusions

The North Water Polynya (NOW) is one of the most productive biological regions in the Arctic with high importance to local and Inuit communities of Nunavut and Greenland (Hastrup et al. 2018; Ribeiro et al. 2021). To provide insights into the potential changes of this region as global temperatures rise, we investigated the physical and biological oceanic responses of the NOW region to <2 °C (low) and >3.5 °C (high) warming using the CESM1 climate model (Sanderson et al. 2017; Kay et al. 2015; Hurrell et al. 2013). We showed that global temperature increases are associated with reduced winter sea ice production, reduced sea ice import and export, accelerated spring sea ice melt, and larger open water areas that are no longer distinct from central Baffin Bay open waters. While the physical changes in the NOW area and ocean properties were found to be linear with warming, we find a non-linear response of the biological productivity in the NOW region. As a result, we define different regimes of biological productivity for different warming levels. For the low warming regime (<2 °C of warming), increased polynya areas and sea ice melt occur alongside increased stratification, isolating surface waters from those at depth, leading to increased concentrations of nutrient-rich West Greenland Irminger Waters (WGIW) throughout the NOW region. In the eastern coastal region of the NOW, the WGIW is able to replenish the surface with nutrients despite the increased stratification, due to upwelling from northerly winds which drive offshore Ekman transport. This balance, alongside a shift in phytoplankton community composition from diatoms to small phytoplankton, leads to an increase in productivity relative to the historical simulation along the Greenlandic coastline in the NOW. Importantly, this shift on phytoplankton distribution can have profound ecosystem impacts despite an increase in productivity. In the coastal regions of the western NOW however, peak productivity remains relatively constant as the deeper and more diluted WGIW is unable to resupply the surface mixed layer under predominantly onshore Ekman transports. For the high warming regime (>3.5 °C of warming), we see even stronger increases in stratification and WGIW presence than at lower warming levels in both western and eastern coastal regions. Despite increased nutrient availability at depth, coastal convection and mixing is unable to counter the increased stratification and bring

those nutrients to the surface. Thus, we find a decreases in biological productivity during all months of the growing season in the NOW in the high warming regime. These results, in concert with the small influence of internal climate variability on these processes, point to the importance of limiting global temperature increases to 2 °C or less in order to avoid the most impactful changes in the NOW ecosystem.

*Acknowledgments.* This study was supported by NSF award 1804504. We also acknowledge NSF CAREER award 1847398, as this manuscript grew out of a project in a Course Based Research experience (CURE) class at CU Boulder taught as part of award 1847398, which also supported the contribution of C. Wyburn-Powell, P. Ugrinow, and R. Patel and the early work on the project by A. Jahn. We would also like to acknowledge high-performance computing on Cheyenne provided by NCAR's Computational and Information Systems Laboratory, sponsored by the National Science Foundation. We thank Thomas Juul-Pedersen for discussions on biogeochemical dynamics in Baffin Bay, Kristen Krumhardt for discussions about NPP in the CESM1, Anna-Marie Strehl for discussions on stratification, and Ivonne Martinez and Patricia DeRepentigny for early exploratory work on the future evolution of the NOW. We thank the reviewers of this paper whose substantive comments greatly improved the manuscript.

*Data availability statement.* Model output from the CESM1 can be found at https://ncar.github.io/cesm-lens-aws/ and https://www2.cesm.ucar.edu/experiments/1.5-2.0-targets.html. Observed sea ice concentrations are available at https://nsidc.org/data/g02202/versions/4. Nares Strait ice area fluxes from 2017 and 2018 (Moore et al. 2021) are available from https://borealisdata.ca/dataset.xhtml?persistentId=doi:10.5683/SP2/WRGX0K. ERA5 winds are available at https://cds.climate.copernicus.eu/datasets/reanalysis-era5-single-levels-monthly-means?tab=download.

## References


Bailey, J. N. L., R. W. Macdonald, H. Sanei, P. M. Outridge, S. C. Johannessen, K. Hochheim, D. Barber, and G. A. Stern, 2013: Change at the margin of the North Water Polynya, Baffin Bay, inferred from organic matter records in dated sediment cores. *Marine Geology*, **341**, 1–13, https://doi.org/10.1016/j.margeo.2013.04.017.

Ballinger, T. J., G. W. K. Moore, Y. Garcia-Quintana, P. G. Myers, A. A. Imrit, D. Topal, and W. N. Meier, 2022: Abrupt Northern Baffin Bay Autumn Warming and Sea-Ice Loss Since the Turn of the Twenty-First Century. *GEOPHYSICAL RESEARCH LETTERS*, **49 (21)**, e2022GL101 472, https://doi.org/10.1029/2022GL101472.

Barber, D., J. Hanesiak, W. Chan, and J. Piwowar, 2001a: Sea-ice and meteorological conditions in Northern Baffin Bay and the North Water polynya between 1979 and 1996. *Atmosphere-Ocean*, **39 (3)**, 343–359, https://doi.org/10.1080/07055900.2001.9649685.

Barber, D., R. Marsden, P. Minnett, G. Ingram, and L. Fortier, 2001b: Physical processes within the North Water (NOW) polynya. *Atmosphere-Ocean*, **39 (3)**, 163–166, https://doi.org/10.1080/07055900.2001.9649673.

Bi, H., Z. Zhang, Y. Wang, X. Xu, Y. Liang, J. Huang, Y. Liu, and M. Fu, 2019: Baffin Bay sea ice inflow and outflow: 1978–1979 to 2016–2017. *The Cryosphere*, **13 (3)**, 1025–1042, https://doi.org/10.5194/tc-13-1025-2019.

Buchart, L., and Coauthors, 2022: Future Climate Scenarios for Northern Baffin Bay and the Pikialasorsuaq (North Water Polynya) Region. *Atmosphere-Ocean*, **0 (0)**, 1–22, https://doi.org/10.1080/07055900.2022.2067028.

Burgers, T. M., L. A. Miller, S. Rysgaard, J. Mortensen, B. Else, J.-E. Tremblay, and T. Papakyriakou, 2023: Distinguishing Physical and Biological Controls on the Carbon Dynamics in a High-Arctic Outlet Strait. *Journal of Geophysical Research: Oceans*, **128 (3)**, e2022JC019 393, https://doi.org/10.1029/2022JC019393.

Castro de la Guardia, L., X. Hu, and P. G. Myers, 2015: Potential positive feedback between Greenland Ice Sheet melt and Baffin Bay heat content on the west Greenland shelf. *Geophysical Research Letters*, **42 (12)**, 4922–4930, https://doi.org/10.1002/2015GL064626.

Day, J. J., M. M. Holland, and K. I. Hodges, 2018: Seasonal differences in the response of Arctic cyclones to climate change in CESM1. *Climate Dynamics*, **50 (9)**, 3885–3903, https://doi.org/10.1007/s00382-017-3767-x.

DeRepentigny, P., A. Jahn, M. M. Holland, and A. Smith, 2020: Arctic Sea Ice in Two Configurations of the CESM2 During the 20th and 21st Centuries. *Journal of Geophysical Research: Oceans*, **125 (9)**, e2020JC016 133, https://doi.org/10.1029/2020JC016133.

Dumont, D., Y. Gratton, and T. E. Arbetter, 2009: Modeling the Dynamics of the North Water Polynya Ice Bridge. *Journal of Physical Oceanography*, **39 (6)**, 1448–1461, https://doi.org/10.1175/2008JPO3965.1.

Dumont, D., Y. Gratton, and T. E. Arbetter, 2010: Modeling Wind-Driven Circulation and Landfast Ice-Edge Processes during Polynya Events in Northern Baffin Bay. *Journal of Physical Oceanography*, **40 (6)**, 1356–1372, https://doi.org/10.1175/2010JPO4292.1.

Dunbar, M., and M. Dunbar, 1972: The history of the North Water. *Proceedings of the Royal Society of Edinburgh, Section B: Biological Sciences*, **72**, 231–241.

DuVivier, A. K., M. M. Holland, J. E. Kay, S. Tilmes, A. Gettelman, and D. A. Bailey, 2020: Arctic and Antarctic Sea Ice Mean State in the Community Earth System Model Version 2 and the Influence of Atmospheric Chemistry. *Journal of Geophysical Research: Oceans*, **125 (8)**, e2019JC015 934, https://doi.org/10.1029/2019JC015934.

Fol, M., B. Tremblay, S. Pfirman, R. Newton, S. Howell, and J.-F. Lemieux, 2025: Revisiting the Last Ice Area projections from a high-resolution Global Earth System Model. *Communications Earth & Environment*, **6 (1)**, 1–12, https://doi.org/10.1038/s43247-025-02034-5.

Georgiadis, E., J. Giraudeau, A. Jennings, A. Limoges, R. Jackson, S. Ribeiro, and G. Massé, 2020: Local and regional controls on Holocene sea ice dynamics and oceanography in Nares Strait, Northwest Greenland. *Marine Geology*, **422**, 106 115, https://doi.org/10.1016/j.margeo.2020.106115.

Gjelstrup, C. V. B., and C. A. Stedmon, 2024: A switch in thermal and haline contributions to stratification in the Greenland Sea during the last four decades. *Progress in Oceanography*, **225**, 103 283, https://doi.org/10.1016/j.pocean.2024.103283.

690 Grønnow, B., 2016: Living at a High Arctic Polynya: Inughuit Settlement and Subsistence around
691 the North Water during the Thule Station Period, 1910–53. *ARCTIC*, **69 (5)**, 1–15, https://doi.org/
692 10.14430/arctic4573.

693 Gutjahr, O., and G. Heinemann, 2018: A model-based comparison of extreme winds in the
694 Arctic and around Greenland. *International Journal of Climatology*, **38 (14)**, 5272–5292,
695 https://doi.org/10.1002/joc.5729.

696 Harning, D. J., B. Holman, L. Woelders, A. E. Jennings, and J. Sepúlveda, 2023: Biomarker
697 characterization of the North Water Polynya, Baffin Bay: implications for local sea ice and
698 temperature proxies. *Biogeosciences*, **20 (1)**, 229–249, https://doi.org/10.5194/bg-20-229-2023.

699 Hastrup, K., A. Mosbech, and B. Grønnow, 2018: Introducing the North Water: Histories of
700 exploration, ice dynamics, living resources, and human settlement in the Thule Region. *Ambio*,
701 **47 (Suppl 2)**, 162–174, https://doi.org/10.1007/s13280-018-1030-2.

702 Hausfather, Z., K. Marvel, G. A. Schmidt, J. W. Nielsen-Gammon, and M. Zelinka, 2022: Climate
703 simulations: recognize the 'hot model' problem. *Nature*, **605 (7908)**, 26–29, https://doi.org/
704 10.1038/d41586-022-01192-2.

705 Heide-Jørgensen, M. P., L. M. Burt, R. G. Hansen, N. H. Nielsen, M. Rasmussen, S. Fossette, and
706 H. Stern, 2013: The Significance of the North Water Polynya to Arctic Top Predators. *AMBIO*,
707 **42 (5)**, 596–610, https://doi.org/10.1007/s13280-012-0357-3.

708 Heide-Jørgensen, M. P., M.-H. S. Sinding, N. H. Nielsen, A. Rosing-Asvid, and R. G. Hansen,
709 2016: Large numbers of marine mammals winter in the North Water polynya. *Polar Biology*,
710 **39 (9)**, 1605–1614, https://doi.org/10.1007/s00300-015-1885-7.

711 Howell, S. E. L., D. G. Babb, J. C. Landy, G. W. K. Moore, T. J. Ballinger, K. McNeil, B. Montpetit,
712 and M. Brady, 2024: Baffin Bay Ice Export and Production From Sentinel-1, the RADARSAT
713 Constellation Mission, and CryoSat-2: 2016–2022. *Geophysical Research Letters*, **51 (22)**,
714 e2024GL111 364, https://doi.org/10.1029/2024GL111364.

715 Howell, S. E. L., D. G. Babb, J. C. Landy, G. W. K. Moore, B. Montpetit, and M. Brady,
716 2023: A Comparison of Arctic Ocean Sea Ice Export Between Nares Strait and the Canadian

Arctic Archipelago. *Journal of Geophysical Research: Oceans*, **128 (4)**, e2023JC019 687, https://doi.org/10.1029/2023JC019687.

Hurrell, J. W., and Coauthors, 2013: The Community Earth System Model: A Framework for Collaborative Research. *Bulletin of the American Meteorological Society*, **94 (9)**, 1339–1360, https://doi.org/10.1175/BAMS-D-12-00121.1.

Jackson, R., and Coauthors, 2021: Holocene polynya dynamics and their interaction with oceanic heat transport in northernmost Baffin Bay. *Scientific Reports*, **11 (1)**, 10 095, https://doi.org/10.1038/s41598-021-88517-9.

Jahn, A., and R. Laiho, 2020: Forced Changes in the Arctic Freshwater Budget Emerge in the Early 21st Century. *Geophysical Research Letters*, **47 (15)**, e2020GL088 854, https://doi.org/10.1029/2020GL088854.

Jeong, H., S.-S. Lee, H.-S. Park, and A. L. Stewart, 2023a: Future changes in Antarctic coastal polynyas and bottom water formation simulated by a high-resolution coupled model. *Communications Earth & Environment*, **4 (1)**, 490, https://doi.org/10.1038/s43247-023-01156-y.

Jeong, H., and Coauthors, 2023b: Southern Ocean polynyas and dense water formation in a high-resolution, coupled Earth system model. *The Cryosphere*, **17 (7)**, 2681–2700, https://doi.org/10.5194/tc-17-2681-2023.

Kanna, N., S. Sugiyama, Y. Ohashi, D. Sakakibara, Y. Fukamachi, and D. Nomura, 2018: Upwelling of Macronutrients and Dissolved Inorganic Carbon by a Subglacial Freshwater Driven Plume in Bowdoin Fjord, Northwestern Greenland. *Journal of Geophysical Research: Biogeosciences*, **123 (5)**, 1666–1682, https://doi.org/10.1029/2017JG004248.

Kay, J. E., and Coauthors, 2015: The Community Earth System Model (CESM) Large Ensemble Project: A Community Resource for Studying Climate Change in the Presence of Internal Climate Variability. *Bulletin of the American Meteorological Society*, **96 (8)**, 1333–1349, https://doi.org/10.1175/BAMS-D-13-00255.1.

Kirillov, S., I. Dmitrenko, D. G. Babb, J. K. Ehn, N. Koldunov, S. Rysgaard, D. Jensen, and D. G. Barber, 2022: The role of oceanic heat flux in reducing thermodynamic ice growth in

Nares Strait and promoting earlier collapse of the ice bridge. *Ocean Science*, **18 (5)**, 1535–1557, https://doi.org/10.5194/os-18-1535-2022.

Koerner, K. A., A. Limoges, N. Van Nieuwenhove, T. Richerol, G. Massé, and S. Ribeiro, 2021: Late Holocene sea-surface changes in the North Water polynya reveal freshening of northern Baffin Bay in the 21st century. *Global and Planetary Change*, **206**, 103 642, https://doi.org/10.1016/j.gloplacha.2021.103642.

Kohnemann, S. H. E., and G. Heinemann, 2025: Gap Flows in Nares Strait: Multi-Scale Numerical Model Simulations in Comparison to Aircraft Measurements. *Earth and Space Science*, **12 (5)**, e2024EA003 912, https://doi.org/10.1029/2024EA003912.

Kwok, R., 2007: Baffin Bay ice drift and export: 2002–2007. *Geophysical Research Letters*, **34 (19)**, https://doi.org/10.1029/2007GL031204.

Kwok, R., L. Toudal Pedersen, P. Gudmandsen, and S. S. Pang, 2010: Large sea ice outflow into the Nares Strait in 2007. *Geophysical Research Letters*, **37 (3)**, https://doi.org/10.1029/2009GL041872.

Laliberté, F., S. E. L. Howell, J.-F. Lemieux, F. Dupont, and J. Lei, 2018: What historical landfast ice observations tell us about projected ice conditions in Arctic archipelagoes and marginal seas under anthropogenic forcing. *The Cryosphere*, **12 (11)**, 3577–3588, https://doi.org/10.5194/tc-12-3577-2018.

Lemieux, J.-F., F. Dupont, P. Blain, F. Roy, G. C. Smith, and G. M. Flato, 2016: Improving the simulation of landfast ice by combining tensile strength and a parameterization for grounded ridges. *Journal of Geophysical Research: Oceans*, **121 (10)**, 7354–7368, https://doi.org/10.1002/2016JC012006.

Marchese, C., C. Albouy, J.-E. Tremblay, D. Dumont, F. D'Ortenzio, S. Vissault, and S. Bélanger, 2017: Changes in phytoplankton bloom phenology over the North Water (NOW) polynya: a response to changing environmental conditions. *Polar Biology*, **40 (9)**, 1721–1737, https://doi.org/10.1007/s00300-017-2095-2.

Marinov, I., S. C. Doney, and I. D. Lima, 2010: Response of ocean phytoplankton community structure to climate change over the 21st century: partitioning the effects of nutrients, temperature and light. *Biogeosciences*, **7 (12)**, 3941–3959, https://doi.org/10.5194/bg-7-3941-2010.

Meier, W. N., J. S. Stewart, F. Fetterer, and A. K. Windnagel, 2021: NOAA/NSIDC Climate Data Record of Passive Microwave Sea Ice Concentration, Version 4. National Snow and Ice Data Center, https://doi.org/10.7265/efmz-2t65.

Melling, H., Y. Gratton, and G. Ingram, 2001: Ocean circulation within the North Water polynya of Baffin Bay. *Atmosphere-Ocean*, **39 (3)**, 301–325, https://doi.org/10.1080/07055900.2001.9649683.

Moore, G. W. K., 2021: Impact of model resolution on the representation of the wind field along Nares Strait. *Scientific Reports*, **11 (1)**, 13 271, https://doi.org/10.1038/s41598-021-92813-9.

Moore, G. W. K., S. E. L. Howell, and M. Brady, 2023: Evolving relationship of Nares Strait ice arches on sea ice along the Strait and the North Water, the Arctic's most productive polynya. *Scientific Reports*, **13 (1)**, 9809, https://doi.org/10.1038/s41598-023-36179-0.

Moore, G. W. K., S. E. L. Howell, M. Brady, X. Xu, and K. McNeil, 2021: Anomalous collapses of Nares Strait ice arches leads to enhanced export of Arctic sea ice. *Nature Communications*, **12 (1)**, 1, https://doi.org/10.1038/s41467-020-20314-w.

Moore, G. W. K., and A. A. Imrit, 2022: Impact of Resolution on the Representation of the Mean and Extreme Winds Along Nares Strait. *Journal of Geophysical Research: Atmospheres*, **127 (19)**, e2022JD037 443, https://doi.org/10.1029/2022JD037443.

Moore, G. W. K., and K. Våge, 2018: Impact of model resolution on the representation of the air–sea interaction associated with the North Water Polynya. *Quarterly Journal of the Royal Meteorological Society*, **144 (714)**, 1474–1489, https://doi.org/10.1002/qj.3295.

Moore, J. K., K. Lindsay, S. C. Doney, M. C. Long, and K. Misumi, 2013: Marine Ecosystem Dynamics and Biogeochemical Cycling in the Community Earth System Model [CESM1(BGC)]: Comparison of the 1990s with the 2090s under the RCP4.5 and RCP8.5 Scenarios. *Journal of Climate*, **26 (23)**, 9291–9312, https://doi.org/10.1175/JCLI-D-12-00566.1.

Mosbech, A., K. L. Johansen, T. A. Davidson, M. Appelt, B. Grønnow, C. Cuyler, P. Lyngs, and J. Flora, 2018: On the crucial importance of a small bird: The ecosystem services of the little auk (Alle alle) population in Northwest Greenland in a long-term perspective. *Ambio*, **47 (2)**, 226–243, https://doi.org/10.1007/s13280-018-1035-x.

Muilwijk, M., T. Hattermann, T. Martin, and M. A. Granskog, 2024: Future sea ice weakening amplifies wind-driven trends in surface stress and Arctic Ocean spin-up. *Nature Communications*, **15 (1)**, 6889, https://doi.org/10.1038/s41467-024-50874-0.

Münchow, A., K. K. Falkner, and H. Melling, 2015: Baffin Island and West Greenland Current Systems in northern Baffin Bay. *Progress in Oceanography*, **132**, 305–317, https://doi.org/10.1016/j.pocean.2014.04.001.

Mysak, L. A., and F. Huang, 1992: A Latent-and Sensible-Heat Polynya Model for the North Water, Northern Baffin Bay. *Journal of Physical Oceanography*, **22 (6)**, 596–608, https://doi.org/10.1175/1520-0485(1992)022⟨0596:ALASHP⟩2.0.CO;2.

Nishii, K., H. Nakamura, and Y. J. Orsolini, 2015: Arctic summer storm track in CMIP3/5 climate models. *Climate Dynamics*, **44 (5)**, 1311–1327, https://doi.org/10.1007/s00382-014-2229-y.

Odate, T., T. Hirawake, S. Kudoh, B. Klein, B. LeBlanc, and M. Fukuchi, 2002: Temporal and spatial patterns in the surface-water biomass of phytoplankton in the North Water. *Deep Sea Research Part II: Topical Studies in Oceanography*, **49 (22)**, 4947–4958, https://doi.org/10.1016/S0967-0645(02)00172-8.

Polyakov, I. V., A. V. Pnyushkov, and E. C. Carmack, 2018: Stability of the arctic halocline: a new indicator of arctic climate change. *Environmental Research Letters*, **13 (12)**, 125 008, https://doi.org/10.1088/1748-9326/aaec1e.

Preußer, A., G. Heinemann, S. Willmes, and S. Paul, 2015: Multi-Decadal Variability of Polynya Characteristics and Ice Production in the North Water Polynya by Means of Passive Microwave and Thermal Infrared Satellite Imagery. *Remote Sensing*, **7 (12)**, 15 844–15 867, https://doi.org/10.3390/rs71215807.

Raghavan, M., and Coauthors, 2014: The genetic prehistory of the New World Arctic. *Science (New York, N.Y.)*, **345 (6200)**, 1255 832, https://doi.org/10.1126/science.1255832.

Rasmussen, T. A. S., N. Kliem, and E. Kaas, 2011: The Effect of Climate Change on the Sea Ice and Hydrography in Nares Strait. *Atmosphere-Ocean*, **49 (3)**, 245–258, https://doi.org/10.1080/07055900.2011.604404.

Ren, H., M. Shokr, X. Li, Z. Zhang, F. Hui, and X. Cheng, 2022: Estimation of Sea Ice Production in the North Water Polynya Based on Ice Arch Duration in Winter During 2006–2019. *Journal of Geophysical Research: Oceans*, **127 (10)**, e2022JC018 764, https://doi.org/10.1029/2022JC018764.

Ribeiro, S., and Coauthors, 2021: Vulnerability of the North Water ecosystem to climate change. *Nature Communications*, **12 (1)**, 4475, https://doi.org/10.1038/s41467-021-24742-0.

Rumyantseva, A., N. Lucas, T. Rippeth, A. Martin, S. C. Painter, T. J. Boyd, and S. Henson, 2015: Ocean nutrient pathways associated with the passage of a storm. *Global Biogeochemical Cycles*, **29 (8)**, 1179–1189, https://doi.org/10.1002/2015GB005097.

Sanderson, B. M., and Coauthors, 2017: Community climate simulations to assess avoided impacts in 1.5 and 2  °C futures. *Earth System Dynamics*, **8 (3)**, 827–847, https://doi.org/10.5194/esd-8-827-2017.

Schmidt, S., and U. Send, 2007: Origin and Composition of Seasonal Labrador Sea Freshwater. *Journal of Physical Oceanography*, **37 (6)**, 1445–1454, https://doi.org/10.1175/JPO3065.1.

Sterlin, J., T. Orval, J.-F. Lemieux, C. Rousset, T. Fichefet, F. Massonnet, and J. Raulier, 2024: Influence of the representation of landfast ice on the simulation of the Arctic sea ice and Arctic Ocean halocline. *Ocean Dynamics*, **74 (5)**, 407–437, https://doi.org/10.1007/s10236-024-01611-0.

Stroeve, J., and D. Notz, 2018: Changing state of Arctic sea ice across all seasons. *Environmental Research Letters*, **13 (10)**, 103 001, https://doi.org/10.1088/1748-9326/aade56.

Tamura, T., and K. I. Ohshima, 2011: Mapping of sea ice production in the Arctic coastal polynyas. *Journal of Geophysical Research: Oceans*, **116 (C7)**, https://doi.org/10.1029/2010JC006586.

Tang, C. C., C. K. Ross, T. Yao, B. Petrie, B. M. DeTracey, and E. Dunlap, 2004: The circulation, water masses and sea-ice of Baffin Bay. *Progress in Oceanography*, **63 (4)**, 183–228, https://doi.org/10.1016/j.pocean.2004.09.005.

Tremblay, J.-E., Y. Gratton, E. C. Carmack, C. D. Payne, and N. M. Price, 2002: Impact of the large-scale Arctic circulation and the North Water Polynya on nutrient inventories in Baffin Bay. *Journal of Geophysical Research: Oceans*, **107 (C8)**, 26–1–26–14, https://doi.org/10.1029/2000JC000595.

Tremblay, J.-E., and Coauthors, 2011: Climate forcing multiplies biological productivity in the coastal Arctic Ocean. *Geophysical Research Letters*, **38 (18)**, https://doi.org/10.1029/2011GL048825.

Vincent, R. F., 2019: A Study of the North Water Polynya Ice Arch using Four Decades of Satellite Data. *Scientific Reports*, **9 (1)**, 20 278, https://doi.org/10.1038/s41598-019-56780-6.

Vincent, R. F., 2020: An Examination of the Non-Formation of the North Water Polynya Ice Arch. *Remote Sensing*, **12 (17)**, 2712, https://doi.org/10.3390/rs12172712.

Wolf, K. K. E., C. J. M. Hoppe, L. Rehder, E. Schaum, U. John, and B. Rost, 2024: Heatwave responses of Arctic phytoplankton communities are driven by combined impacts of warming and cooling. *Science Advances*, **10 (20)**, eadl5904, https://doi.org/10.1126/sciadv.adl5904.

Yao, T., and C. L. Tang, 2003: The formation and maintenance of the North Water Polynya. *Atmosphere-Ocean*, **41 (3)**, 187–201, https://doi.org/10.3137/ao.410301.

Zanowski, H., A. Jahn, and M. M. Holland, 2021: Arctic Ocean Freshwater in CMIP6 Ensembles: Declining Sea Ice, Increasing Ocean Storage and Export. *Journal of Geophysical Research: Oceans*, **126 (4)**, e2020JC016 930, https://doi.org/10.1029/2020JC016930.

# Supplementary figures to: Future Sea Ice-Ocean and Biological Productivity Changes in the North Water Polynya Region under Policy Relevant Warming Levels

Jed Lenetsky[1], Alexandra Jahn[1], Patrick Ugrinow[1], Christopher Wyburn-Powell[1], Rajan Patel[1], and Hannah Zanowski[2]

[1]Department of Atmospheric and Oceanic Sciences and Institute of Arctic and Alpine Research, University of Colorado - Boulder, Boulder, Colorado, USA

[2]Department of Atmospheric and Oceanic Sciences, University of Wisconsin-Madison, Madison, Wisconsin, USA

June 24, 2025

| Warming Level | Mean | Maximum | Minimum |
|---|---|---|---|
| **Low warming** | 1.95°C | 2.04°C | 1.88° |
| **High warming** | 4.22°C | 4.89°C | 3.52° |

Table S1: 30 year ensemble mean, ensemble maximum, and ensemble minimum global temperature anomalies for low warming and high warming levels.

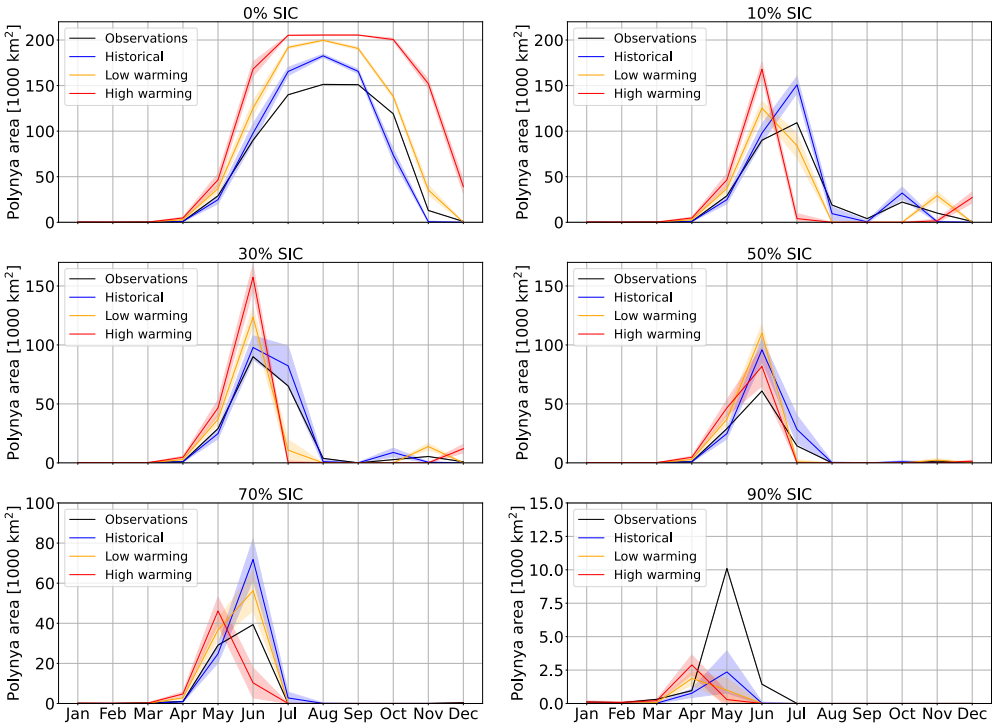


Figure S1: Influence of the SIC threshold choice for when the NOW polynya ceases to exist due to becoming part of Baffin Bay open water (using the southern box shown in Fig. 3) on the seasonal cycle of the polynya for observations (1980-2009; black), CESM1-LE historical (1980-2009; blue), low warming (yellow), and high warming (red) levels. Shading indicates ± 1-standard deviation from the ensemble mean. Note the different y axis limits.

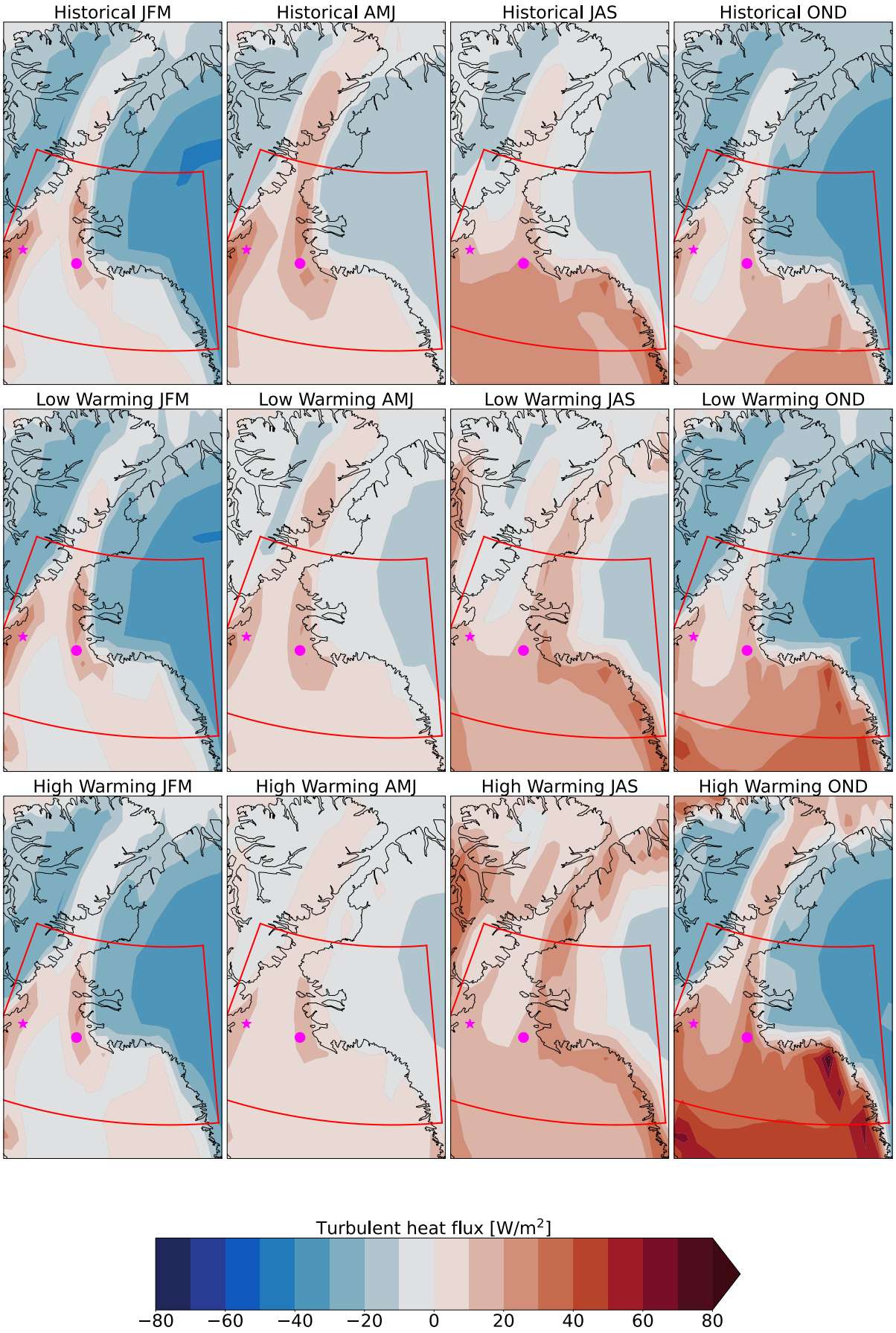


Figure S2: Seasonal cycle of turbulent heat fluxes (latent + sensible) over the NOW region (red box) during the CESM1-LE historical period (1980-2009), and low warming, and high warming levels for winter (JFM), spring (AMJ), summer (JAS) and fall (OND). Positive fluxes are atmospheric heat gain.

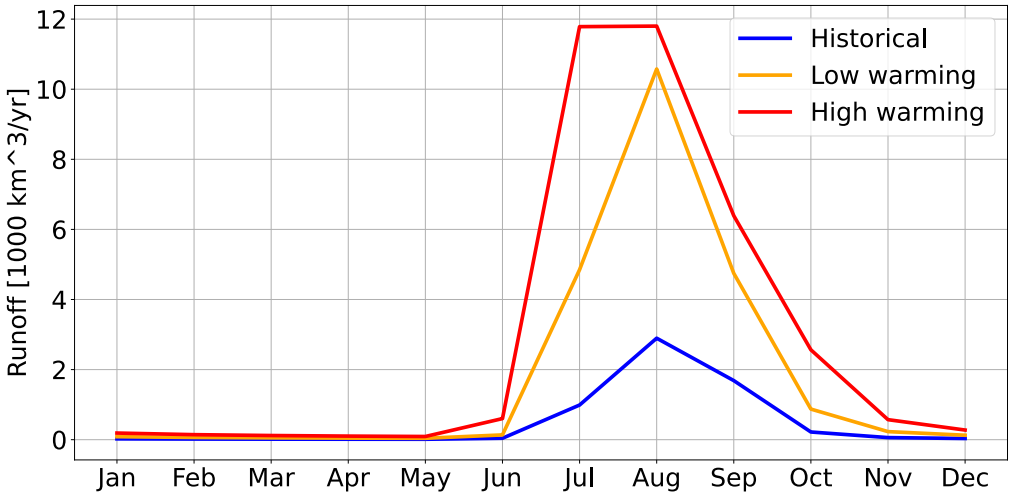


Figure S3: Seasonal cycle of total simulated runoff into the NOW domain (see Fig. 3) for historical (blue), low (orange), and high (red) warming levels.